Check for updates

Original research article

Cell-free therapy for alopecia via the secretome of hiPSC-derived dermal papilla cells

Journal of Tissue Engineering
Volume 17: 1–23
© The Author(s) 2026
Article reuse guidelines:
sagepub.com/journals-permissions
DOI: 10.1177/20417314261449597
journals.sagepub.com/home/tej
Sage

Hyesoo Hwangbo[1,2*], Aoyang Pu[1,2*], Wanyu Tan[1,2*], Eunice Dotse[1,2], Huanhuan Sun[1,2], Xin Gan[1,2], Yun-Gwi Park[3], Yimin Lai[1,2], Soon-Jung Park[3], Inho Choi[4], In-Rok Oh[5], Kwan Ting Chow[1,2], Sung-Hwan Moon[3], Hae-Won Kim[6,7,8,9], Byung Cheol Park[10] and Kiwon Ban[1,2]

Abstract

Alopecia is highly prevalent and debilitating, yet current drugs provide limited, reversible benefit with notable side effects. We established a rapid protocol to generate human induced pluripotent stem cell–derived dermal papilla cells (hiPSC-DPCs) and demonstrated that their conditioned medium (CM) acts as a potent, cell-free hair-regenerative therapy. Transdermal delivery of hiPSC-DPCs or CM accelerated anagen re-entry and hair regrowth in depilated mice, and hiPSC-DPC CM outperformed minoxidil in promoting ex vivo hair-shaft elongation and in vitro proliferation and migration of primary DPCs and keratinocytes. Proteomic and metabolomic profiling revealed enrichment of growth factors, antioxidants, and immunomodulatory metabolites linked to TNF and PI3K–Akt signaling, conferring superior anti-inflammatory and cytoprotective properties relative to primary DPC CM. Moreover, hiPSC-DPC CM mitigated dihydrotestosterone (DHT)-induced pathology by suppressing androgen receptor expression and nuclear translocation. These findings position hiPSC-DPC secretome as a dual-functional, regenerative, and anti-androgenic biologic with translational potential for durable alopecia treatment.

Keywords

alopecia, human induced pluripotent stem cells, dermal papilla cells, secretome, hair regeneration

Received: 19 January 2026; accepted: 27 April 2026

[1]Department of Biomedical Sciences, City University of Hong Kong, Kowloon, China
[2]Tung Biomedical Sciences Centre, City University of Hong Kong, Kowloon, China
[3]Department of Animal Biotechnology, College of Biotechnology and Natural Resources, Chung-Ang University, Anseong, Republic of Korea
[4]Department of Pharmaceutical Engineering, Hoseo University, Asan, Republic of Korea
[5]R&D Center, Qstem Co. Ltd, Anseong, Republic of Korea
[6]Institute of Tissue Regeneration Engineering (ITREN), Dankook University, Cheonan, Republic of Korea
[7]Department of Nanobiomedical Science & BK21 NBM Global Research Center for Regenerative Medicine, Dankook University, Cheonan, Republic of Korea
[8]Department of Biomaterials Science, School of Dentistry, Dankook University, Cheonan, Republic of Korea
[9]Mechanobiology Dental Medicine Research Center, Dankook University, Cheonan, Republic of Korea
[10]Department of Dermatology, College of Medicine, Dankook University, Cheonan-si, Republic of Korea

*These authors contributed equally to this work.

Corresponding authors:
Kiwon Ban, Department of Biomedical Sciences, City University of Hong Kong, Kowloon, Hong Kong China.
Email: ban.kw@cityu.edu.hk

Hae-Won Kim, Institute of Tissue Regeneration Engineering (ITREN), Dankook University, Cheonan 31116, Republic of Korea.
Email: kimhw@dku.edu

Byung Cheol Park, Department of Dermatology, College of Medicine, Dankook University, Cheonan-si 31116, Republic of Korea.
Email: 4exodus@daum.net

Sung-Hwan Moon, Department of Animal Biotechnology, College of Biotechnology and Natural Resources, Chung-Ang University, Anseong 17546, Republic of Korea.
Email: moonsh@cau.ac.kr

Creative Commons Non Commercial CC BY-NC: This article is distributed under the terms of the Creative Commons Attribution-NonCommercial 4.0 License (https://creativecommons.org/licenses/by-nc/4.0/) which permits non-commercial use, reproduction and distribution of the work without further permission provided the original work is attributed as specified on the SAGE and Open Access pages (https://us.sagepub.com/en-us/nam/open-access-at-sage).

Introduction

Alopecia is a common and distressing disorder that affects hundreds of millions of individuals worldwide, leading to profound psychological and social consequences such as diminished self-esteem, anxiety, and social withdrawal. Although not life-threatening, its impact on quality of life is severe, highlighting the need for safe and effective therapeutic solutions.[1] Alopecia encompasses several distinct clinical entities, including androgenetic alopecia (AGA), alopecia areata, and telogen effluvium, each arising from diverse genetic, hormonal, immune, and environmental mechanisms. Among these, AGA—the most prevalent form—is driven primarily by androgen-dependent follicular miniaturization mediated by dihydrotestosterone (DHT).[2]

Despite decades of research, therapeutic options remain extremely limited. Minoxidil and finasteride, the two sole U.S Food and Drug Administration (FDA)–approved drugs for AGA, only offer modest efficacy and reversible benefits. Continuous application is required to sustain hair growth, and withdrawal leads to relapse. Moreover, minoxidil can cause scalp irritation, and finasteride's systemic hormonal effects can result in sexual dysfunction.[3,4] Surgical transplantation procedures provide cosmetic improvement but are invasive, costly, and restricted by donor hair follicle (HF) availability.[5] Collectively, these constraints underscore an urgent unmet need for next-generation, mechanism-based therapies that can restore the intrinsic regenerative competence of HFs while minimizing adverse effects.

Dermal papilla cells (DPCs), specialized mesenchymal cells residing at the base of the HF, serve as the principal signaling center controlling HF morphogenesis and cyclic regeneration.[6] Through the secretion of diverse growth factors, extracellular vesicles (EVs), and regulatory molecules, DPCs coordinate epithelial–mesenchymal interactions (EMIs) that sustain follicular stem cell activation and hair shaft renewal.[7] However, progressive deterioration of DPC function—driven by aging, inflammation, or hormonal dysregulation—has emerged as a key pathogenic mechanism underlying alopecia.[8] Loss of hair-inductive signaling, disrupted crosstalk with epithelial cells, and a decaying secretory profile collectively impair follicle regeneration. Specifically, in AGA, DPCs become miniaturized and transcriptionally suppressed by DHT, leading to follicular atrophy and chronic hair loss.[9] Similar declines in DPC vitality occur in other alopecic conditions, underscoring their indispensable role in follicle homeostasis.[10] Consequently, maintaining a robust supply of functional DPC is vital for hair restoration strategies. Yet, DPCs rapidly lose hair-inductive capacity during conventional in vitro expansion, restricting their therapeutic applicability.[11] Efforts to restore primary DPC potency using three-dimensional culture or molecular reprograming have achieved partial recovery but remain limited by variability, scalability, and immunocompatibility.[12–14]

Human induced pluripotent stem cells (hiPSCs) represent an inexhaustible and ethically acceptable cell source capable of generating patient-specific DPCs that overcome the limitations of primary donor scarcity, senescence, and immune incompatibility. By reprograming mature somatic cells into a pluripotent state, hiPSCs enable the production of autologous, disease-free DPCs on demand, offering a reproducible and potentially standardized platform for regenerative hair loss therapies. Recent studies have demonstrated that hiPSC-derived DPCs (hiPSC-DPCs) are capable of initiating HF morphogenesis when combined with epidermal components, confirming their partial recapitulation of native DPC function.[15–17] However, the differentiated cells often exhibit heterogeneous phenotypes, incomplete transcriptional maturation, and diminished inductive strength compared with primary DPCs, leading to variable and suboptimal hair regeneration in vivo. Moreover, to achieve stable large-scale production of functionally competent hiPSC-DPCs, the current approaches remain technically demanding and time-intensive, which commonly involve embryoid body (EB) culture and require over 1 month of maintenance. Emerging evidence suggests that many of the regenerative effects traditionally attributed to cell engraftment are, in fact, mediated by secreted components that modulate the follicular microenvironment.[14,18,19] The hiPSC-DPC secretome—comprising soluble growth factors, cytokines, EVs, and metabolic regulators—may therefore represent the primary effector responsible for promoting EMIs and restoring follicular cycling. Despite this, the paracrine potential of hiPSC-DPCs has remained largely unexplored, given the difficulty in generating qualified cells efficiently. Characterizing and harnessing this potent secretome could transform hiPSC-based strategies from a cell-dependent model to a safe, scalable, and cell-free therapeutic platform for alopecia.

Here, we developed a rapid, 8-day differentiation protocol to derive functionally competent hiPSC-DPCs and established their conditioned medium (CM) as a potent, cell-free biologic for alopecia therapy. hiPSC-DPC CM promoted robust hair regeneration in depilated mice and stimulated hair shaft elongation in ex vivo follicle cultures, surpassing the performance of minoxidil. Multi-omics analyses revealed that its enriched secretome activates TNF- and PI3K–Akt–dependent regenerative pathways while suppressing DHT-induced androgen-receptor signaling, thereby reversing the core pathology of AGA (Graphical abstract).

Collectively, our findings define a dual-acting, regenerative, and anti-androgenic mechanism mediated by the hiPSC-DPC secretome and establish a scalable, cell-free therapeutic platform for treating alopecia. By coupling the safety of a biologic formulation with the potency of developmental reprograming, this strategy addresses the central limitations of existing pharmacologic and cell-based approaches and represents a promising step toward durable hair restoration.

Results

Rapid generation of hiPSC-DPCs via modulated neural crest-mesenchymal differentiation

Dermal papilla cells (DPCs) are a specialized subset of mesenchymal stem cells (MSCs) located at the base of hair follicles (HFs), and their embryonic origin depends on their anatomical site.[7] Developmental studies have shown that DPCs in the trunk and back derive from the mesoderm, whereas those in the face and scalp originate from the neural crest (NC) via a neuroectodermal lineage.[15,20,21] Building on these observations, we adapted previously established protocols for NC differentiations[22] and DPC induction[15] from human embryonic stem cells (hESCs), and developed a streamlined, 8-day stepwise protocol to generate hiPSC-derived DPCs (hiPSC-DPCs; Figure 1(a)).

To first direct hiPSCs toward a neuroectodermal fate for NC generation, we applied dual Suppressor of Mothers against Decapentaplegic (SMAD) inhibition, which is known to favor neuroectoderm specification.[23] Specifically, we treated hiPSCs with the Bone Morphogenetic Protein (BMP) pathway inhibitor LDN193189 and the TGF-β signaling inhibitor SB431542. After 24 h, qPCR analysis revealed a marked upregulation of the neuroectoderm marker SOX1 (Supplemental Figure 1(a)). Continued culture for 3 days in medium supplemented with epidermal growth factor (EGF) and basic fibroblast growth factor (bFGF) further promoted specification to the NC stage and enhanced cell migration, proliferation, and survival.[22,24] By day 4, the cells robustly expressed NC markers, including AP2α, P75, and SOX9, in contrast to undifferentiated hiPSCs (Supplemental Figure 1(b)).

Because primary DPCs possess a hybrid identity characterized by both MSC and NC features, we incorporated a subsequent 4-day MSC priming phase using a xeno-free medium containing 5% human platelet lysate (HPL) and 20 ng/mL bFGF (Figure 1(a)). Following this priming, hiPSC-DPCs exhibited a substantial increase in the MSC surface markers CD44, CD73, and CD105, reaching levels comparable to those of human primary DPCs (hDPCs) and exceeding those of undifferentiated hiPSCs and hiPSC-NCs (Figure 1(b)). Flow cytometry further confirmed strong protein-level expression of CD44, CD73, and CD90, with more than 88% of hiPSC-DPCs expressing all three markers, mirroring their distribution in hDPCs (Supplemental Figure 1(c)). Immunocytochemistry co-staining for the mesenchymal structural proteins α-smooth muscle actin (SMA) and vimentin, together with the NC marker nestin, demonstrated their abundant presence in hiPSC-DPCs (Figure 1(c)). Together, these findings demonstrate that our 8-day differentiation protocol efficiently generates hiPSC-DPCs that recapitulate the MSC-related characteristics of hDPCs.

hiPSC-DPCs displayed an exceptional hair-inductive profile

It is well established that primary hDPCs readily lose hair-inductive capacity under conventional culture conditions.[25,26] Therefore, despite the similarity between primary hDPCs and hiPSC-DPCs in terms of MSC and NC marker expression, we further examined the expression of hair-inductive markers in hiPSC-DPCs to obtain initial evidence of their trichogenic potential.

qPCR analysis of a panel of genes associated with hair inductivity, including CD133, Versican, alkaline phosphatase (ALP), and β-catenin, revealed significantly higher expression of all these markers in hiPSC-DPCs compared with primary hDPCs (Figure 1(d)–(g)). Notably, CD133 levels were approximately 10,000-fold higher in hiPSC-DPCs than in hDPCs. Given the critical role of CD133 in initiating HF formation in vivo,[27] we performed western blotting (WB), which confirmed robust CD133 protein expression in hiPSC-DPCs, whereas CD133 was undetectable in hDPCs (Figure 1(h) and (i)). Versican, an extracellular matrix (ECM) component that is specifically expressed during the anagen phase of hair growth,[28,29] was also markedly elevated in hiPSC-DPCs relative to hDPCs. In addition, quantification of ALP-positive cells and total ALP protein content demonstrated significantly higher ALP activity in hiPSC-DPCs (Figure 1(j) and (k)) ALP is considered an important indicator that correlates with the trichogenicity of DPCs, and its overexpression has been shown to enhance the hair-inductive capacity of cultured DPCs.[30,31] Additionally, since primary DPCs are known for their ability to self-assemble into 3D structures in vitro, we compared 3D spheroids formed by hDPCs and hiPSC-DPCs and observed that hiPSC-DPC spheroids formed more rapidly and were more compact (Supplemental Figure 2). Extracellular matrix (ECM) derived from DPCs also acts as an instructive niche during the active (anagen) phase of HF growth. Using immunocytochemistry, we found that hiPSC-DPCs strongly expressed two key ECM components, fibronectin and versican (Supplemental Figure 3), which have been documented to play essential roles in mediating hair follicle stem cell (HFSC) behavior during hair regeneration. Together, these findings suggest that hiPSC-DPCs possess a strong molecular signature supportive of hair induction.

Given this superior molecular profile, we hypothesized that hiPSC-DPCs could accelerate hair regrowth in depilated mice via direct transdermal injection. Consistent with this hypothesis, hiPSC-DPCs–treated mice exhibited markedly earlier and denser hair regrowth 10 days after administration, outperforming the minoxidil-treated group, whereas untreated mice retained large areas of hairless skin (Figure 1(l)). Collectively, these data demonstrate that

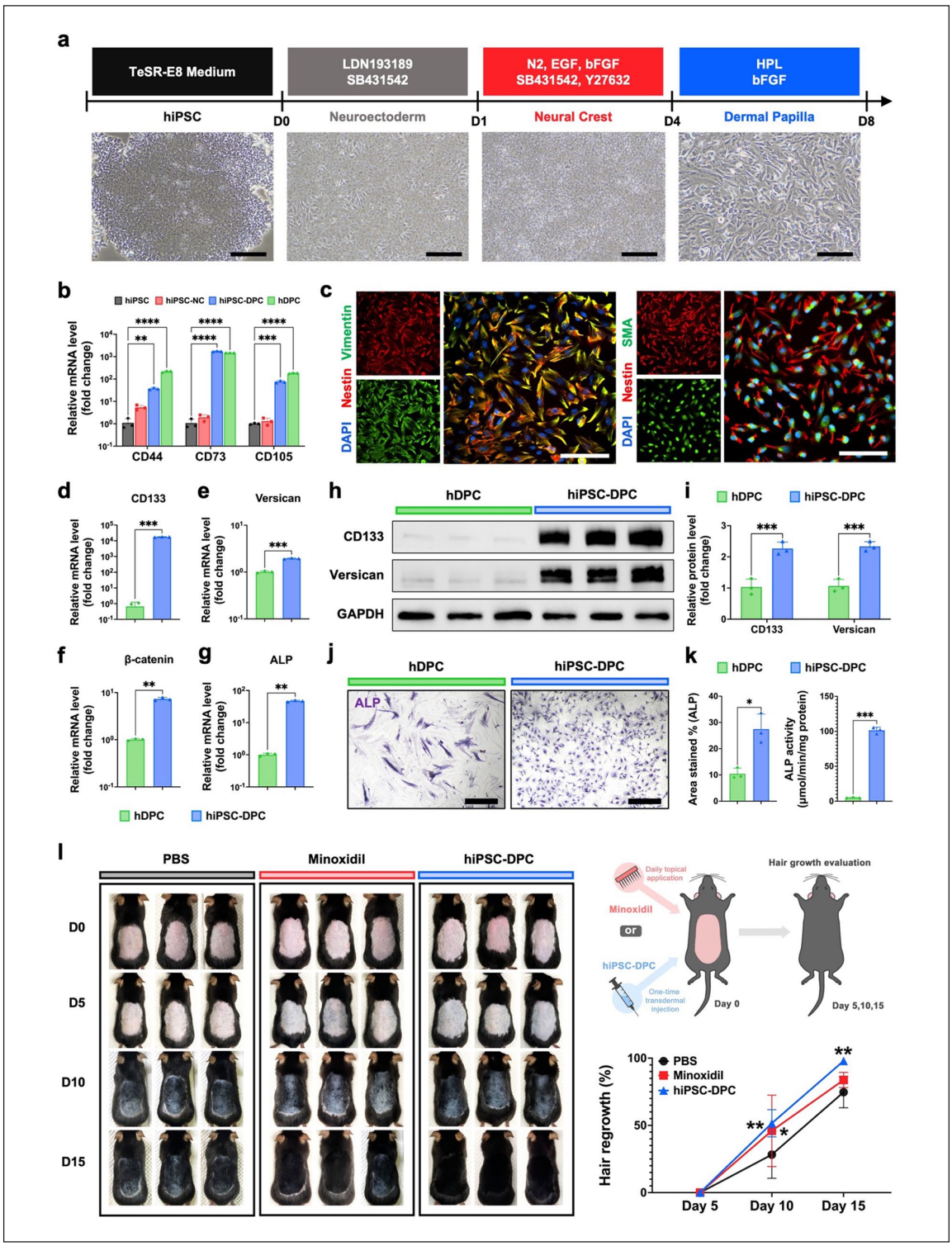


Figure 1. hiPSC-DPCs displayed exceptional hair inductive signatures. (a) Schematic illustrating an 8-day protocol used for differentiating hiPSCs to dermal papilla cells via neural crest lineage, along with the morphological changes observed at each stage of differentiation. Scale bar = 200 μm. (b) qPCR analyzed the increase in MSC markers, including CD44, CD73, and CD105 after hiPSC-DPC differentiation. $^{**}p < 0.01$, $^{***}p < 0.001$, $^{****}p < 0.0001$ versus hiPSC group. $n = 3$. (c) Immunocytochemistry results of neural stem cell marker Nestin and MSC structural markers SMA and Vimentin, expressed in hiPSC-DPCs. Scale bar = 100 μm. (d–g) qPCR analyzed hair-inducing markers CD133, Versican, ALP, and β-catenin expression in hiPSC-DPCs. $^{**}p < 0.01$, $^{***}p < 0.001$ versus hDPC group. $n = 3$. (h and i) Western blot analysis of the protein levels of CD133 and Versican in hDPCs and hiPSC-DPCs. $^{***}p < 0.001$ versus hDPC group. $n = 3$. (j and k) ALP staining and ALP activity assays evaluated ALP levels in hiPSC-DPCs. $^{*}p < 0.05$, $^{***}p < 0.001$ versus hDPC group. $n = 3$. Scale bar = 500 μm. (l) Transdermal injection of hiPSC-DPCs promoted hair recovery in C57BL/6 mice after depilation, and minoxidil was included as a positive control. $^{*}p < 0.05$, $^{**}p < 0.01$ versus PBS group. $n = 5$.

8-day–generated hiPSC-DPCs display superior hair-inductive activity compared with primary hDPCs.

hiPSC-DPC CM rejuvenated human follicular cells in vitro

HF morphogenesis and cycling critically depend on cross-talk between epithelial keratinocytes (KCs) and hair-inductive mesenchymal DPCs. Although direct cell–cell contact contributes to this interaction, HF formation and sustained shaft elongation are primarily driven by DPC-derived secreted factors.[14,18,19] To examine the impact of the hiPSC-DPC secretome on hair regrowth, we collected conditioned medium (CM) from hiPSC-DPCs cultured for 48 h in serum-free basal medium (Figure 2(a)). ALP activity was used as a quantitative marker for quality control, as it linearly correlated with both hair-inductive gene expression in hiPSC-DPCs and the proliferative potential of the resulting CM (Supplemental Figure 4).

We first evaluated the effects of hiPSC-DPC–derived CM on human HF-related cells including human primary DPCs (hDPCs) and KCs (hKCs). hDPCs were treated with 10%, 20%, or 50% CM derived from either hDPCs or hiPSC-DPCs. After 48 h, hiPSC-DPC CM enhanced ALP staining intensity in a dose-dependent manner (Figure 2(b) and (c)), whereas hDPC CM failed to induce noticeable changes even at the highest concentration, which may partly account for its diminished efficacy during in vitro expansion. Quantification of intracellular ALP activity in hDPCs confirmed an approximately 2-fold increase starting at 10% hiPSC-DPC CM (Figure 2(d)).

In addition to ALP, proliferative potential is a key indicator of DPC functional vigor. CCK-8 assays showed increased cell density of hDPCs following hiPSC-DPC CM treatment (Figure 2(e)). This pro-proliferative effect became prominent only after prolonged exposure (72–96 h), likely reflecting the senescent phenotype and reduced responsiveness of primary hDPCs.

We then examined the impact of hiPSC-DPC CM on hKCs, whose behavior closely reflects HF growth or suppression.[32] Notably, hiPSC-DPC CM induced a significant increase in hKC proliferation within 48 h, a more rapid response than that observed in hDPCs (Figure 2(f)). Immunocytochemical staining for the proliferation marker Ki67 further demonstrated an approximately 3-fold increase in Ki67-positive hKCs following treatment with 20% hiPSC-DPC CM (Figure 2(g) and (h)). Moreover, the transwell migration assay revealed that CM-treated hKCs displayed significantly greater migratory areas than untreated controls (Figure 2(i) and (j)), indicating that factors present in hiPSC-DPC CM markedly enhanced hKC activity. Because hair shaft elongation primarily depends on the continuous proliferation and upward movement of newly generated hKCs within the HF, these findings suggest that hiPSC-DPC CM rejuvenates the cellular function of both HF-associated DPCs and KCs, thereby supporting robust hair elongation and regrowth. In addition, we investigated the potential therapeutic effects of hiPSC-DPC CM on skin-related cells, including immortalized human keratinocytes (HaCaT) and human dermal fibroblasts (hDFs), given their suitability for large-scale culture. Migration assays using scratch and transwell protocols for HaCaT cells and hDFs, respectively, revealed significantly enhanced migratory activity after 24–72 h of hiPSC-DPC CM treatment (Supplemental Figures 5 and 6). These data suggest a broad role for hiPSC-DPC CM in rejuvenating both hair- and skin-related cells toward a more youthful state. Importantly, DPCs derived from hiPSCs exhibit a vigorous secretory profile that supports active hair follicle growth, whereas aged and senescent DPCs produce reduced levels of growth factors, thereby impairing HF development and contributing to hair thinning and loss. CM obtained from hiPSC-DPCs, which maintain a developmentally youthful and functionally robust phenotype, contains elevated levels of hair regeneration–associated growth factors compared to CM from primary DPCs and other HF-associated cells. Therefore, hiPSC-DPC–derived CM may represent a promising cell-free strategy for hair regeneration.

Given that the AKt/GSK-3β pathway is a well-established signaling cascade controlling hair growth through the regulation of follicular cell proliferation, we treated primary hDPCs and hKCs with 20% or 50% hiPSC-DPC CM, followed by WB analysis of pathway components. Among both cell types we tested, hiPSC-DPC CM induced a clear, dose-dependent increase in AKt phosphorylation (p-AKt) without markedly altering total AKt levels (Figure 2(k) and (l)), indicating bona fide pathway activation rather than changes in protein abundance. In parallel, we observed increased phosphorylation of GSK3 (p-GSK3), a key downstream effector of AKt. Because phosphorylated GSK3 is inactivated, this modification is expected to reduce β-catenin degradation, favoring its cytoplasmic accumulation and nuclear translocation. This mechanism aligns well with prior reports that the β-catenin–GSK3 axis in DPCs plays a central role in controlling HFSC activity and anagen entry.[14,33] However, further WB analysis of hDPCs and hKCs treated with hiPSC-DPC CM did not reveal significant changes in β-catenin expression (Supplemental Figure 7), suggesting a β-catenin-independent mechanism underlying CM-activated PI3K–AKt signaling, potentially involving noncanonical *Wnt* ligands that mediate HFSC activity and hair regeneration.[34]

hiPSC-DPC CM accelerated hair growth ex vivo and in vivo

Having established the potent hair-inductive activity of hiPSC-DPC CM in vitro, we next evaluated its functional effects on human and mouse HFs as a preclinical assessment (Figure 3(a)). In the mouse vibrissa HF organ culture

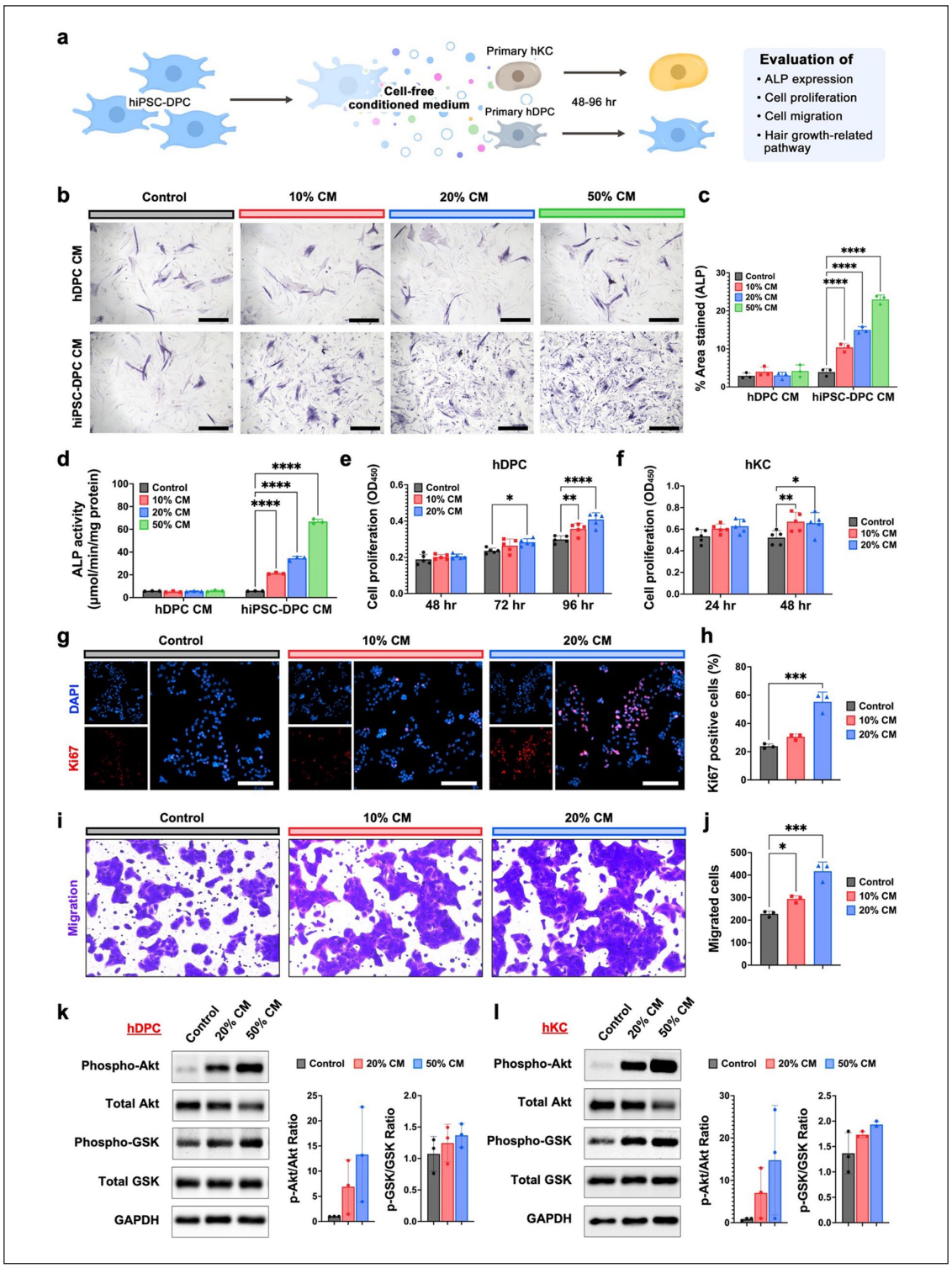


Figure 2. hiPSC-DPC CM activated human follicular cells in vitro. (a) Schematic illustrating that hiPSC-DPC CM rejuvenates primary human follicular cells, including hDPCs and hKCs. (b–d) hiPSC-DPC CM enhanced ALP activities of primary hDPCs, demonstrated by a colorimetric ALP staining assay and quantitative ALP activity assay. $^{****}p < 0.0001$ versus control group. $n = 3$. Scale bar = 500 μm. (e and f) hiPSC-DPC CM promoted cell proliferation of hDPCs and hKCs, respectively, evaluated by CCK-8 assay. $^{*}p < 0.05$, $^{**}p < 0.01$, $^{****}p < 0.0001$ versus control group. $n = 5$. (g and h) Immunocytochemical staining of proliferative cell marker Ki67 expression in hKCs after administration of hiPSC-DPC CM. $^{**}p < 0.001$ versus control group. $n = 3$. Scale bar = 100 μm. (i and j) Transwell migration assay assessed cell migration of hKCs after hiPSC-DPC CM treatment. $^{*}p < 0.05$, $^{**}p < 0.001$ versus control group. $n = 3$. Scale bar = 200 μm. (k and l) Western blotting analyzed phosphorylation of Akt and GSK in hDPCs and hKCs after hiPSC-DPC CM treatment. $n = 3$.

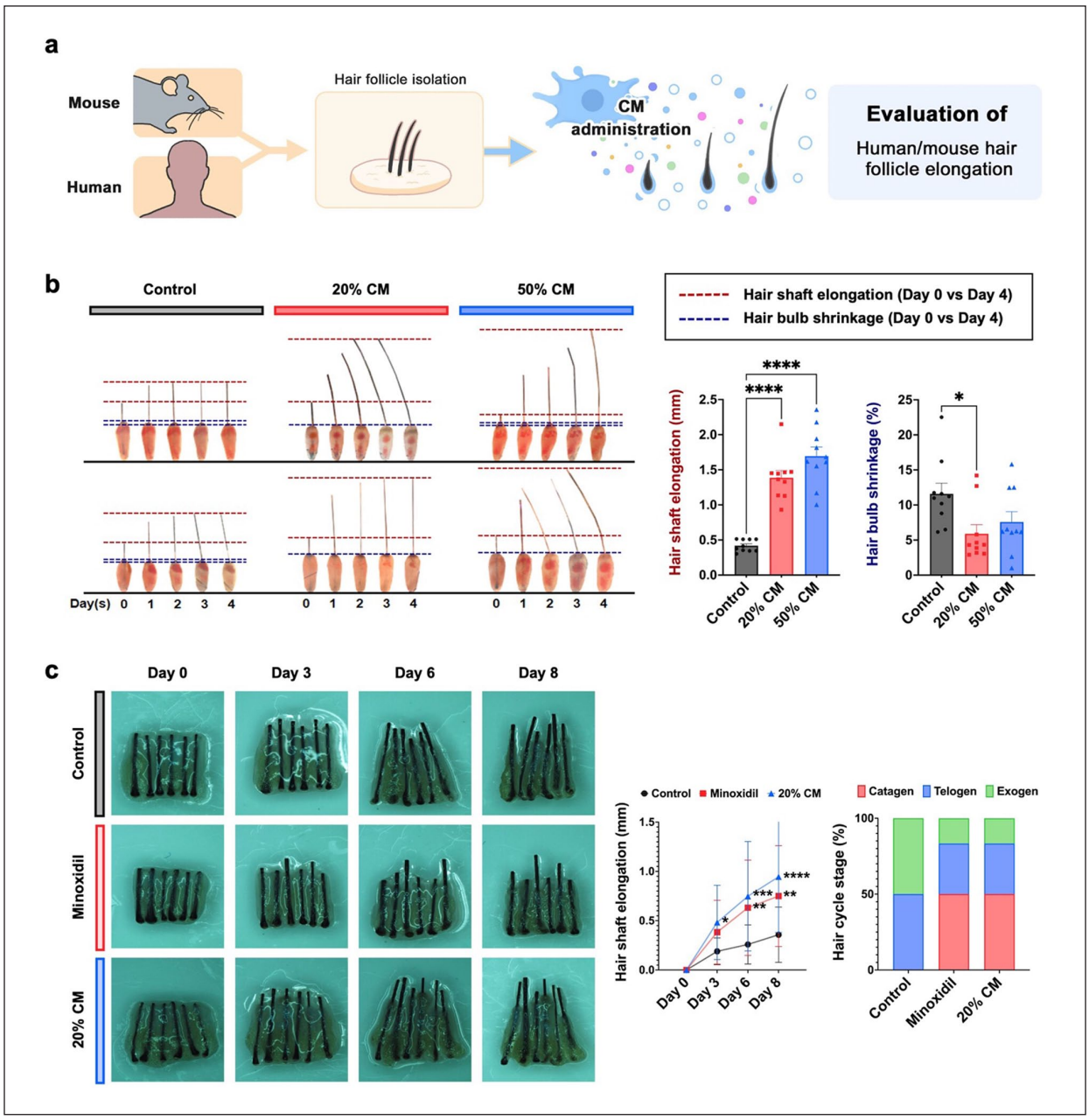


Figure 3. hiPSC-DPC CM promoted hair shaft elongation of ex vivo isolated human and mouse hair follicles. (a) Schematic illustrating the effect of hiPSC-DPC CM on ex vivo mouse vibrissae and human hair follicles. (b) hiPSC-DPC CM accelerated the growth of the mouse vibrissa hair follicle, followed by quantification of the hair shaft elongation and hair bulb dimension. Red dotted lines indicate hair shaft elongation; blue dotted lines denote hair bulb dimension changes. *$p < 0.05$, ****$p < 0.0001$ versus control group. $n = 10$. (c) Sequential photograph of human hair follicles cultured with vehicle control, 20 μM minoxidil, and 20% hiPSC-DPC CM for 8 days, followed by quantification of hair shaft elongation and hair cycles from each group at day 8 were classified based on morphological appearances. *$p < 0.05$ versus control group. $n = 17$.

model, hiPSC-DPC CM significantly promoted HF elongation in a dose-dependent manner: 20% CM and 50% CM induced average daily length increases of 0.347 and 0.423 mm, respectively (Figure 3(b)) Moreover, HFs treated with hiPSC-DPC CM exhibited sustained, visible growth over the entire observation period, whereas control follicles showed growth arrest by day 3. Because shrinkage of the hair bulb is a characteristic indicator of entry into catagen,[35] we further assessed HF morphology. Follicles exposed to hiPSC-DPC CM preserved intact structures, with hair bulbs retaining more than 88% of the total HF length. These findings indicate that hiPSC-DPC

CM rapidly enhances HF elongation without compromising follicular integrity, supporting the potential biosafety of hiPSC-DPC CM during application.

To assess whether these effects from hiPSC-DPC CM could be sustained in a preclinical condition, we isolated human HFs from donors and randomly assigned them to different treatment groups. As a result, hiPSC-DPC CM significantly promoted the sprouting and elongation of human HFs beginning on day 3, with sustained growth observed up to day 8 (Figure 3(c)). Notably, hiPSC-DPC CM treatment resulted in ~26% greater net elongation than minoxidil by day 8. Minoxidil also exerted a pro-growth effect; however, HF elongation in the minoxidil group was delayed, with a smaller net increase in length, and growth ceased after day 6. We further analyzed HF cycling status to distinguish anagen, catagen, telogen, and exogen stages in treated follicles. The distribution of catagen, telogen, and exogen phases was comparable between the hiPSC-DPC CM and minoxidil groups, whereas control follicles displayed a higher proportion of telogen and exogen follicles. Catagen and telogen correspond to resting or regressive states, and exogen represents the shedding phase of the hair cycle.[36] Collectively, these data indicate that hiPSC-DPC CM accelerates human HF elongation and supports the generation of structurally robust hair shafts that are more resistant to transition into regressive and shedding phases.

Given the pronounced ex vivo effects and absence of obvious adverse changes, we next investigated the in vivo efficacy of hiPSC-DPC CM by topically applying it to depilated dorsal skin of mice (Figure 4(a)). By day 6, visible hair emergence was evident in mice treated with hiPSC-DPC CM, whereas skins treated with PBS, hDPC CM, or minoxidil showed minimal or no change. By day 10, minoxidil-treated mice displayed a comparable hair-covered area; however, the hiPSC-DPC CM group exhibited more densely packed and darker hair coverage (Figure 4(b) and (c)). In contrast, hDPC CM unexpectedly failed to produce similar benefits, which may reflect functional decline of primary hDPCs during in vitro culture. Consistently, H&E staining revealed longer and more compact HFs in skin from the hiPSC-DPC CM–treated group compared with controls (Figure 4(d)–(f)).

Proteomic analysis of hiPSC-DPC CM reveals activation of the PI3K/Akt pathway

To dissect the mechanisms by which hiPSC-DPC CM promotes hair growth, we performed an in-depth, label-free quantitative proteomic comparison of CM from hiPSC-DPCs and primary hDPCs. Principal component analysis (PCA) revealed a clear segregation between the two secretomes, indicating a substantial shift in the overall protein repertoire. Notably, hiPSC-DPC CM formed a distinct cluster that accounted for 93.48% of the variance in protein composition (PC1: 89.86%, PC2: 3.62%; Figure 5(a)), suggesting that reprograming and directed differentiation endow hiPSC-DPCs with a unique, hair-favorable secretory profile. Unsupervised hierarchical clustering and Venn diagram analysis further underscored extensive differences between the two groups, with hiPSC-DPC CM displaying broad upregulation of a panel of hair-relevant and regenerative proteins (Figure 5(b) and (c)). Among them, we identified increased secretion of platelet-derived growth factor subunit A (PDGFA), PWP1, histone deacetylase 3 (HDAC3), Jagged1 (JAG1), nuclear factor κB subunit 1 (NFκB1), fibroblast growth factor 7 (FGF7), interleukin-1 receptor type 1 (IL1R1), mechanistic target of rapamycin (MTOR), and FADD. Many of these molecules are established regulators of stem cell activity, epithelial–mesenchymal crosstalk, and tissue regeneration,[37–39] suggesting that hiPSC-DPCs secrete a more "regenerative" cocktail than their primary counterparts.

Gene Ontology (GO) enrichment analysis of upregulated proteins highlighted biological processes linked to positive chemotaxis, DNA-dependent ATPase activity, and growth factor activity (Figure 5(d)). Functionally, these categories are consistent with the enhanced migration, proliferation, and anabolic activity we observed in primary hDPCs and hKCs exposed to hiPSC-DPC CM (Figure 2(b)–(j)). This alignment between molecular signatures and functional outcomes supports the notion that hiPSC-DPC CM actively rejuvenates otherwise senescent or functionally compromised follicular cells, shifting them toward a younger, HF-supportive phenotype.

KEGG pathway enrichment further revealed significant activation of signaling pathways critical for cell survival, growth, and redox homeostasis, including TNF signaling, glutathione metabolism, PI3K/Akt signaling, thyroid hormone synthesis, and ECM–receptor interaction (Figure 5(e)). Among these, the TNF and PI3K/Akt axes are particularly intriguing in the context of hair biology. TNF produced by macrophages has been reported to activate *Wnt* signaling in HFSCs, thereby initiating hair regeneration.[40] Moreover, TNF can promote β-catenin accumulation in HFs through an AKt-dependent but *Wnt*-independent route, and pharmacological inhibition of PI3K/AKt signaling leads to arrested hair growth in depilated mice.

These converging lines of evidence led us to hypothesize that hiPSC-DPC CM enhances PI3K/AKt activity in HF-associated cell populations—including hDPCs, hKCs, and hDFs—resulting in the potentiation of hair induction.

Collectively, these proteomic data strongly support a model in which hiPSC-DPC CM delivers a coordinated set of secreted factors that converge on TNF and PI3K/AKt signaling, thereby activating canonical β-catenin–related programs in hair-associated cells. This signaling cascade likely underpins the robust revitalization of DPCs and KCs and the enhanced hair induction observed ex vivo and in vivo.

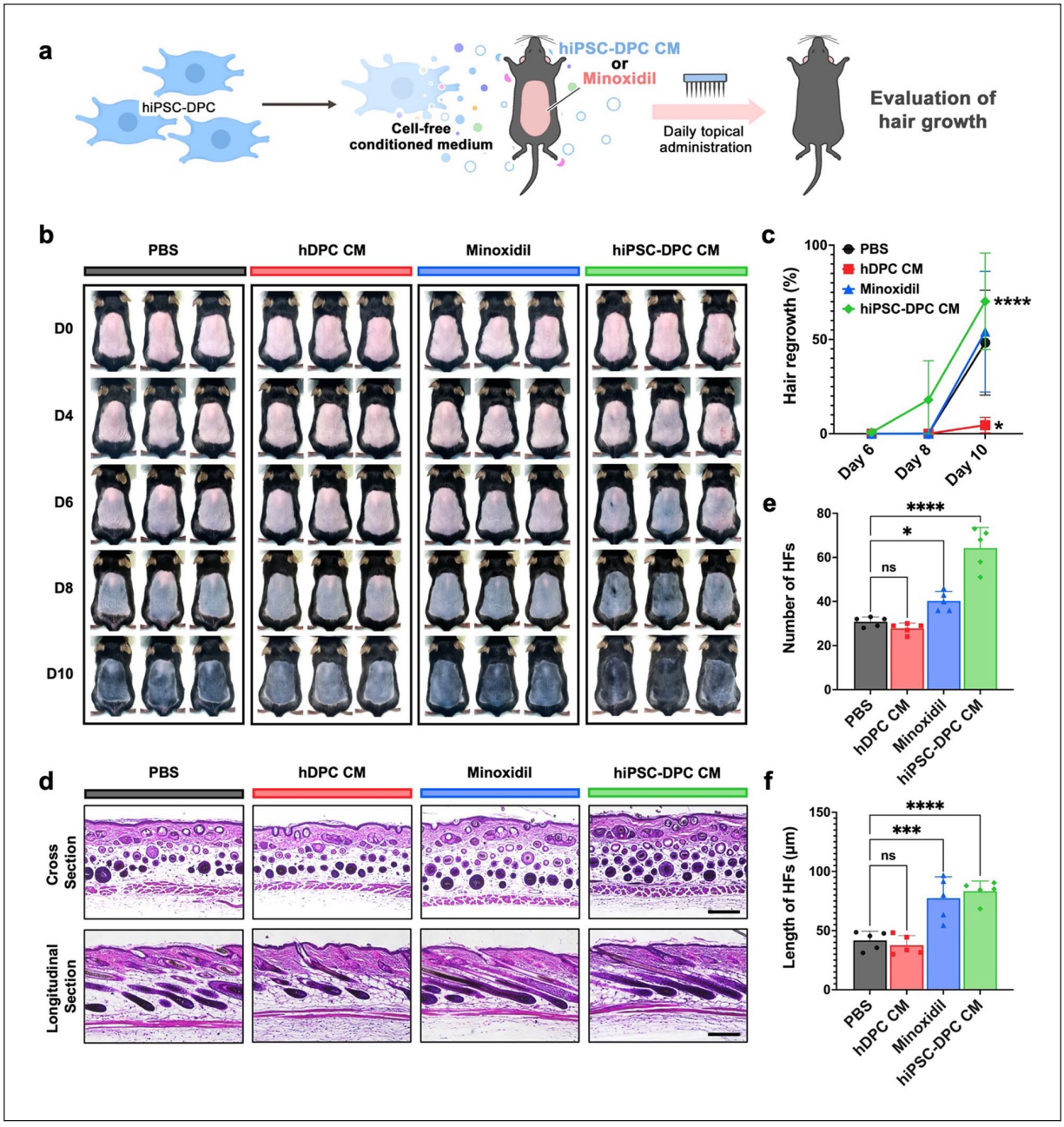


Figure 4. hiPSC-DPC CM facilitated hair regrowth in vivo. (a) Scheme depicts hiPSC-DPC CM application facilitates hair regrowth in vivo. (b and c) Topical administration of hiPSC-DPC CM accelerated hair recovery of depilated C57BL/6 mice, and PBS, hDPC CM, and minoxidil were included as controls, followed by quantification of the area with hair coverage. *$p < 0.05$, ****$p < 0.0001$ versus PBS group. $n = 5$. (d–f) H&E staining analysis of hair follicle (HF) density and length from dorsal skin samples after hiPSC-DPC CM treatment. *$p < 0.05$, ***$p < 0.001$, ****$p < 0.0001$ versus PBS group. $n = 5$. Scale bar = 200 μm.

Metabolomic analysis indicates strengthened antioxidant and glutamine metabolism in hiPSC-DPC CM

Beyond proteins, low-molecular-weight metabolites are increasingly recognized as critical regulators of stem cell fate, tissue regeneration, and hair cycling. For example, glutamine metabolism has been shown to maintain HFSC progenitor states and to generate neogenic cues that promote de novo HF formation.[41] To determine whether metabolic differences also contribute to the superior hair-promoting effects of hiPSC-DPC CM, we performed untargeted metabolomic profiling and compared its metabolite composition with CM from primary hDPCs obtained from two donors.

Strikingly, we observed a consistent enrichment of glutamine metabolism in hiPSC-DPC CM relative to both

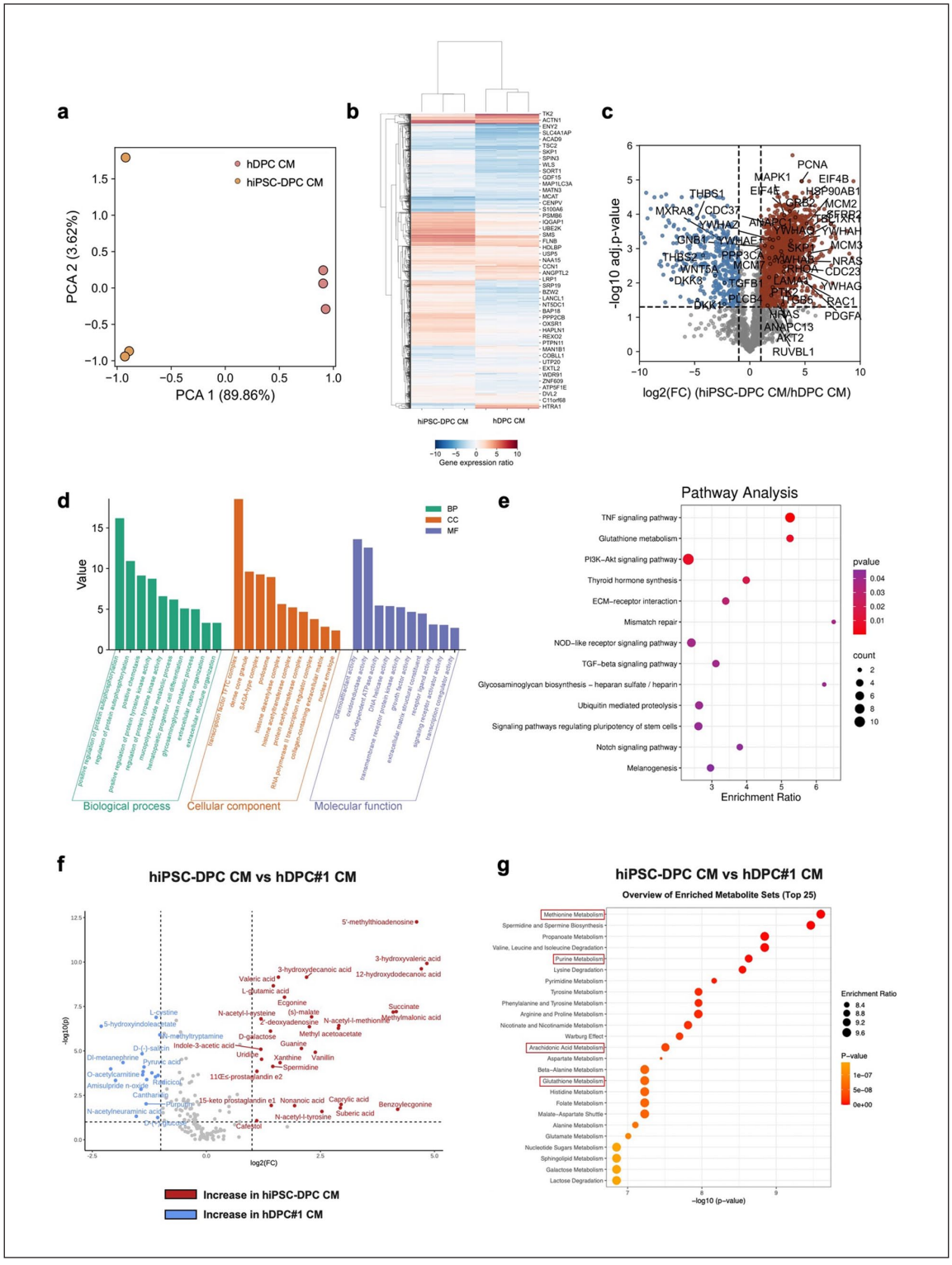


Figure 5. Multi-omics analysis revealed up-regulated hair inductive pathways of hiPSC-DPC CM. (a) Principal component analysis (PCA) analysis of proteomics revealed distinct protein expression of hiPSC-DPC CM and hDPC CM samples. (b) Heatmap and cluster analysis of hiPSC-DPC CM and hDPC CM. (c) Volcano plot analysis between hiPSC-DPC CM and hDPC CM (Fold change threshold: 2; *p*-value threshold by FDR method: 0.05). (d) Gene ontology (GO) analysis of hiPSC-DPC CM versus hDPC CM showed enriched terms in biological processes, cellular components, and molecular functions in DEPs, differentially expressed proteins. (e) Functional classes enrichment analysis of hiPSC-DPC CM versus hDPC CM DEPs using KEGG annotations. (f and g) Metabolomics of Volcano plot of differentiated metabolites and enriched metabolite sets of SMPDB analysis between CM from hiPSC-DPC and hDPC#1.

hDPC#1 and hDPC#2 (Figure 5(f) and (g), and Supplemental Figure 8). This suggests not only increased availability of glutamine itself but also upregulation of associated pathways that fuel nucleotide synthesis, anaplerosis, and redox balance—processes essential for rapidly proliferating and regenerating cells such as HFSCs and matrix keratinocytes. In line with our proteomic findings (Figure 5(e)), we also detected significant upregulation of glutathione-related metabolites, pointing to an enhanced antioxidant microenvironment in hiPSC-DPC CM.

Glutathione represents a central cellular antioxidant, and its depletion is known to exacerbate reactive oxygen species (ROS) accumulation and trigger apoptosis. In addition to glutathione, several other metabolic pathways involved in ROS detoxification and redox homeostasis—including methionine, purine, and arachidonic acid metabolism—were specifically enriched in hiPSC-DPC CM (Figure 5(f) and (g), and Supplemental Figure 8). These metabolic signatures indicate that hiPSC-DPC CM is not only pro-regenerative but also actively anti-oxidative.

This is particularly relevant to hair biology, as mounting evidence shows that chronic or excessive ROS can drive DPC senescence, impair HFSC function, and contribute to hair thinning and loss during aging or under pathological scalp conditions. Conversely, antioxidant interventions have been reported to strengthen HF defenses, rescue senescent DPCs and HFSCs, and restore more physiological hair cycling dynamics.[42,43]

Taken together, our metabolomic data suggest that hiPSC-DPC CM provides a metabolically favorable niche characterized by enhanced glutamine flux and robust antioxidant capacity. When integrated with our proteomic findings—especially the activation of TNF and PI3K/AKt signaling—these results support a unified model in which hiPSC-DPC CM: (i) Rejuvenates hair-related cells (DPCs, KCs, and HFSCs) through pro-growth, pro-migration, and survival signals; (ii) Stabilizes β-catenin signaling via AKt-mediated GSK3 inactivation, thereby promoting anagen entry and maintenance; and (iii) Protects follicles from oxidative damage by reinforcing glutathione and ROS-scavenging pathways, preserving HF integrity and prolonging functional hair production. This combined proteomic–metabolomic landscape positions hiPSC-DPC CM as a potent, multifactorial, and mechanistically rational candidate for hair regeneration therapies.

hiPSC-DPC CM promoted hair regeneration through additional antioxidant and anti-inflammatory effects

To assess the anti-ROS competence, we co-treated primary hDPCs with hiPSC-DPC CM and ROS inducer H_2O_2 (Figure 6(a)). Cell viability assay suggested that H_2O_2 triggered approximately 50% cell death, which was significantly prevented in the presence of CM, achieving almost equivalent cell survival as healthy controls (Figure 6(b)). DCFDA assay, a fluorescent indicator that detects cellular oxidation, was employed to determine intracellular ROS. As expected, hiPSC-DPC CM greatly inhibited H_2O_2-induced ROS, showing the absence of excited signals. Notably, the ROS intensity of the CM-administrated group was unexpectedly lower than control that did not involve any external oxidative stimulus (Figure 6(c) and (d)), suggesting that hiPSC-DPC CM rapidly counteracted the burst of ROS and maintained a vigorous state of hDPC.

DPPH, a stable free radical centralized with nitrogen, was further employed to evaluate the comprehensive role of hiPSC-DPC CM in eliminating ROS. As a result, the inhibition of DPPH in the hiPSC-DPC CM-administered groups was significant, where violet-colored DPPH free radical changed to a colorless and yellow form (Supplemental Figure 9). Notably, the scavenging effect from hiPSC-DPC CM was enhanced when the concentration increased from 30% to 50%, with a reduction of approximately 60% and 90% production of the DPPH, respectively (Figure 6(e)). In addition, hiPSC-DPC CM presented a dose-dependent outcome on DPPH reduction starting from 20%, and nearly dispelled circumambient DPPH with only 50% of CM (Figure 6(f)). Given the promising effects of hiPSC-DPC CM on eliminating ROS, we speculated that hiPSC-DPC CM could also prevent ROS accumulation in ex vivo HFs, thereby maintaining their viability and capacity for continued growth after isolation (Figure 3). To evaluate the off-the-shelf efficacy of CM, we used either solution- or powder-form CM preserved at room temperature (RT), based on the premise that metabolites are more stable than proteins. As expected, both RT-preserved hiPSC-DPC CM solution and powder reduced ROS levels in ex vivo–maintained mouse HFs (Supplemental Figure 10), supporting the robust anti-ROS capacity of hiPSC-DPC CM in preventing tissue-level oxidative stress.

Other than ROS, inflammation also adversely alters hair growth and disrupts hair cycles by delivering immune-mediated cytokines to HF.[44] Given proteomic evidence revealing several immune-related pathways enriched in hiPSC-DPC CM such as TNF and TGF-β signaling (Figure 5(e)), we speculated that hiPSC-DPC CM could prime immune cells (e.g. macrophages) to release HF-favorable cytokines and promote hair regrowth. To achieve this, we carried out a membrane-based inflammatory-cytokine array, where human macrophages were incubated with hiPSC-DPC CM and supernatant were collected to determine the relative levels of targeted cytokines and chemokines (Figure 6(g)). As a result, a total of 11 cytokines showed differentially expressed cytokine levels, among which 5 cytokines (APOA1, PDGFA/PDGFB, DPP4, IL10 and CXCL10) increased after CM treatment, while other 6 cytokines, (MIF, LIF, CD14, MPO, CXCL5 and VEGFA) displayed decreased intensity (Figure 6(h)–(k)). Notably, APOA1 and IL10 were considered as

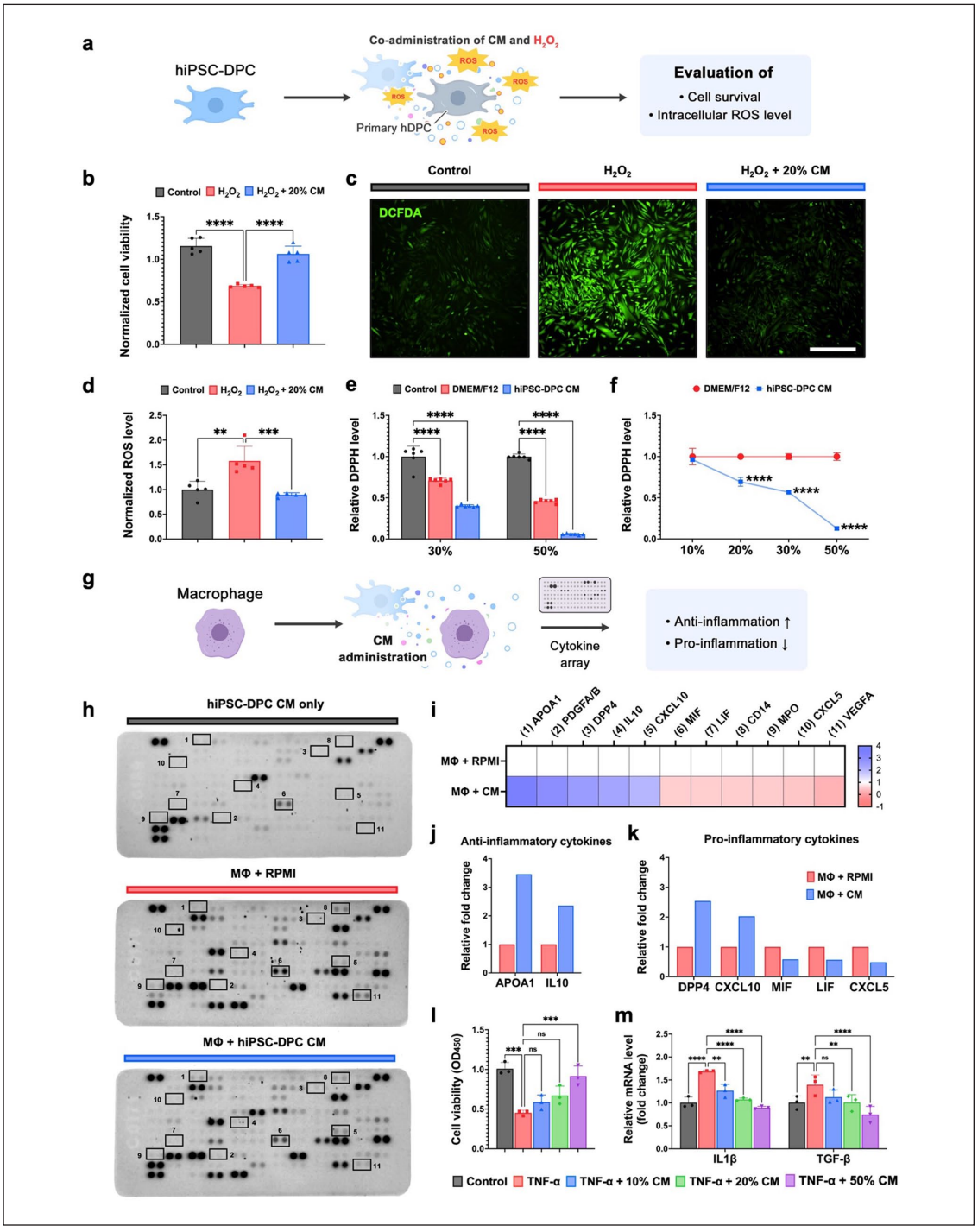


Figure 6. Antioxidative and anti-inflammatory activities of hiPSC-DPC CM. (a) Schematic diagram depicts the protocol of co-administrating hiPSC-DPC CM and H_2O_2 to investigate the antioxidant potential of CM. (b) 20% hiPSC-DPC CM alleviated H_2O_2-induced cell death of hDPCs, and cell viability was assessed using CCK-8 assay. ****$p < 0.0001$ versus H_2O_2-treated groups. $n = 5$. (c and d) Representative images showed intracellular ROS levels after co-administration of hiPSC-DPC CM and H_2O_2, the ROS level was determined by DCFDA ROS assay, followed by quantification summary. **$p < 0.01$, ***$p < 0.001$ versus H_2O_2-treated groups. $n = 5$. Scale bar = 500 μm. (e and f) hiPSC-DPC CM scavenged DPPH free radicals, which was evaluated using the DPPH assay. ****$p < 0.0001$ versus control group. $n = 6$. (g) Schematic diagram shows the effects of hiPSC-DPC CM on human macrophages. (h) Inflammatory cytokine array profiled the cytokine difference from human macrophages with or without hiPSC-DPC CM treatment. (i) Heatmap of differentially expressed cytokines from cytokine array ($|\log_2 FC| \geq 1$). (j and k) Relative fold change of anti-inflammatory and pro-inflammatory cytokines released from hiPSC-DPC CM-treated macrophages (l) CCK-8 assay suggested that hiPSC-DPC CM prevented TNF-α induced cell death of hKCs. **$p < 0.01$, ***$p < 0.001$ versus TNF-α group. $n = 3$. (m) qPCR analyzed inhibited pro-inflammatory gene expressions in TNF-α treated hKCs after hiPSC-DPC CM treatment. **$p < 0.01$, ****$p < 0.0001$ versus TNF-α group. $n = 3$.

anti-inflammatory cytokines, while DPP4, CXCL10, MIF, LIF, and CXCL5 have been reported for their pro-inflammatory outcomes.[45–47] Despite the increase in DPP4 and CXCL10, the downregulation of MIF, LIF, and CXCL5 and the upregulation of APOA1 and IL10 suggested an overall anti-inflammatory potential of hiPSC-DPC CM by regulating immune cells.

To obtain direct evidence of anti-inflammatory effects of hiPSC-DPC CM on HF and hair-related cells, we co-administrated CM and inflammation inducer TNF-α on hKCs. Cell viability results showed that hiPSC-DPC CM inhibited TNF-α-triggered cell death with a dose-dependent effect, where 50% CM resulted in nearly 100% survival (Figure 6(l)). qPCR analyses were conducted to evaluate specific cytokines mediating the protection. As a result, pro-inflammatory cytokines, including IL1β and TGF-β, were significantly downregulated in CM-treated hKCs, while other cytokines were not detected across all the groups (Figure 6(m)).

hiPSC-DPC CM inhibits DHT-induced nuclear translocation of androgen receptor (AR)

Androgenetic alopecia (AGA) is the most prevalent form of hair loss and is primarily driven by excessive androgen signaling, particularly testosterone and dihydrotestosterone (DHT). These androgens bind to the androgen receptor (AR) in DPCs, promote progressive miniaturization of HFs, and ultimately lead to hair loss.[2] To determine whether hiPSC-DPC CM can mitigate AGA-like pathology and achieve therapeutically relevant protection and regeneration, we established DHT-based cellular and HF models (Figure 7(a)).

Since ALP activity is a key indicator of DPC hair inductivity and cellular "youthfulness," we first examined ALP level in primary hDPCs co-treated with DHT and hiPSC-DPC CM. Despite the presence of DHT, hiPSC-DPC CM preserved its rejuvenating capacity, inducing more than a 2-fold increase in ALP activity at both 20% and 50% CM (Figure 7(b)–(d)), whereas hDPC CM had no detectable effect. Notably, DHT itself did not reduce baseline ALP activity but attenuated the magnitude of the hiPSC-DPC CM effect, as ALP induction was substantially higher under non-DHT conditions (~7-fold, Figure 2(b)). These findings suggest that the hDPCs used were relatively senescent and largely unresponsive to DHT, yet remained amenable to functional rejuvenation by hiPSC-DPC CM.

Although these primary hDPCs had lost robust folliculogenicity and showed diminished ALP, they retained proliferative capacity during expansion. We observed that DHT significantly impaired hDPC proliferation, an effect that was prevented by 20% hiPSC-DPC CM (Figure 7(e)). Strikingly, treatment with 50% hiPSC-DPC CM not only rescued DHT-induced growth inhibition but further increased cell density beyond untreated controls, indicating that hiPSC-DPC CM can both salvage DHT-damaged cells and drive DPCs toward a more proliferative, youthful state.

Given that AR activation and nuclear translocation in DPCs are central to AGA pathogenesis, we next sought to delineate the mechanistic basis of hiPSC-DPC CM–mediated protection. qPCR analysis revealed that brief exposure to hiPSC-DPC CM reduced AR mRNA levels in DHT-treated hDPCs, with modest differences between 20% and 50% CM relative to controls (Figure 7(f)), consistent with partial "primitivization" of hDPCs toward a lower-AR–expressing state. To more precisely assess AR localization, we performed immunocytochemistry for AR in hDPCs. As expected, DHT treatment induced pronounced nuclear translocation of AR, shifting the signal from a predominantly cytoplasmic distribution to a nuclear pattern. In contrast, cells treated with 20% or 50% hiPSC-DPC CM retained strong AR staining within the cytoplasm, with a marked reduction in nuclear accumulation (Figure 7(g) and (h)). These data indicate that hiPSC-DPC CM effectively prevents DHT-induced AR nuclear translocation in hDPCs, thereby interrupting a key pathogenic step in AGA and limiting AR-driven senescent signaling.

To evaluate the translational relevance of these findings, we employed an ex vivo model of DHT-challenged HFs. We assessed both functional (hair shaft elongation) and structural (hair bulb morphology) outcomes. DHT exposure induced a rapid shift to catagen within 2 days, characterized by epithelial–mesenchymal dissociation, hair shaft detachment, growth arrest, and bulb atrophy. Quantification of hair bulb diameter demonstrated pronounced shrinkage, with only 69.7% of the original bulb size retained, consistent with hair-cycle arrest (Figure 7(i)–(k)). In contrast, treatment with hiPSC-DPC CM restored and further enhanced HF elongation and preserved bulb integrity. HFs treated with 20% and 50% hiPSC-DPC CM retained 89.4% and 94.5% of bulb diameter, respectively, and continued to grow under DHT challenge.

Together, these results demonstrate that hiPSC-DPC CM can (i) sustain or restore DPC youthfulness and proliferative capacity in a DHT-rich environment, (ii) prevent DHT-induced AR nuclear translocation in hDPCs, and (iii) protect whole HFs from DHT-driven catagen transition and bulb miniaturization. These findings highlight the strong therapeutic potential of hiPSC-DPC CM for counteracting DHT-induced AGA.

Discussion

Dermal papilla cells (DPCs), specialized mesenchymal stem cells (MSCs) residing at the base of hair follicles (HFs), are key orchestrators of follicular morphogenesis and cyclic regeneration through epithelial–mesenchymal signaling. Their secretory output nourishes the follicular niche that sustains keratinocyte proliferation, stem-cell

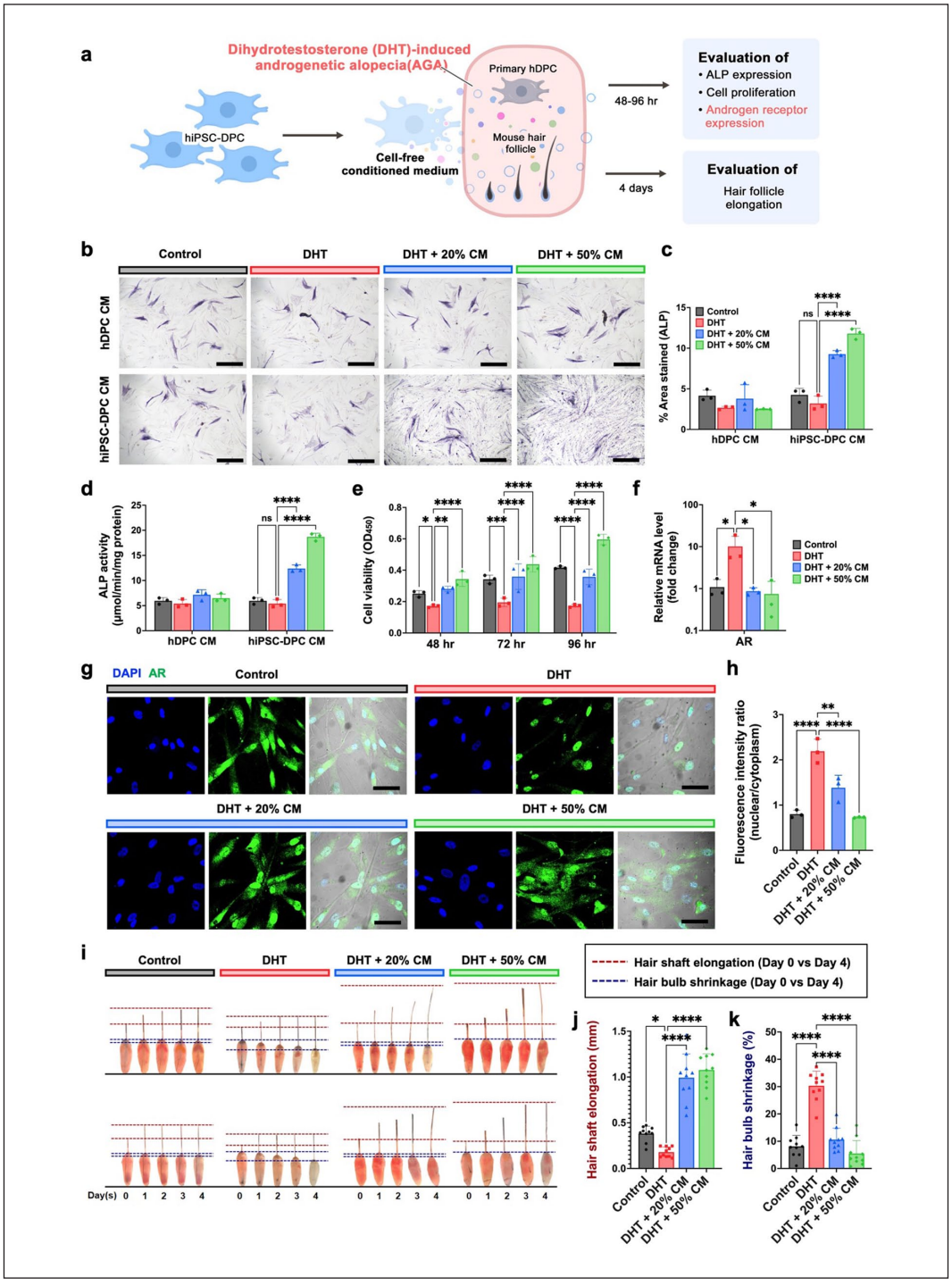


Figure 7. hiPSC-DPC CM safeguarded hair growth in a DHT-induced androgenetic alopecia (AGA). (a) Scheme illustrates the protocol of examining anti-AGA effects from hiPSC-DPC CM in vitro and ex vivo. (b–d) hiPSC-DPC CM promoted ALP activities of dihydrotestosterone (DHT)-damaged hDPCs, demonstrated by a colorimetric ALP staining assay and quantitative ALP activity assay. ****$p < 0.0001$ versus DHT group. $n = 3$. Scale bar = 100 μm. (e) hiPSC-DPC CM enhanced cell proliferation of DHT-treated hDPCs, evaluated by CCK-8 assay. *$p < 0.05$, **$p < 0.01$, ***$p < 0.001$, ****$p < 0.0001$ versus DHT group. $n = 3$. (f) qPCR analyzed that hiPSC-DPC CM inhibited androgen receptor (AR) expression of DHT-treated hDPCs. *$p < 0.05$ versus DHT group. $n = 3$. (g and h) Immunolabels of AR in DHT-treated hDPCs with or without hiPSC-DPC CM administration, followed by a quantification summary comparing the fluorescence intensity of AR among groups. $n = 3$. **$p < 0.01$, ****$p < 0.0001$ versus DHT group. Scale bar = 50 μm. (i–k) Representative images with quantification summary demonstrated that hiPSC-DPC CM counteracted DHT-driven ex vivo hair follicle regression. Red dotted lines indicated hair shaft elongation; blue dotted lines denoted changes in hair bulb dimensions (day 0 vs day 4). $n = 10$. *$p < 0.05$, ****$p < 0.0001$ versus DHT group.

activation, and matrix remodeling. However, DPC regenerative capacity gradually declines under genetic, hormonal, or environmental stress, resulting in impaired paracrine signaling and loss of follicular maintenance.[48] In androgenetic alopecia (AGA), for instance, dihydrotestosterone (DHT) represses DPC transcriptional activity and induces miniaturization, resulting in progressive follicular regression. Functional deterioration of DPCs thus constitutes a central pathogenic mechanism shared across multiple forms of hair loss.

Harnessing the DPC secretome—the repertoire of bioactive molecules driving epithelial–mesenchymal communication—has emerged as a promising, cell-free approach to stimulate hair regeneration. Despite compelling conceptual appeal, practical barriers have limited its therapeutic translation. Primary DPCs are scarce and labor-intensive to harvest, rapidly lose hair-inductive potential during in vitro expansion, and exhibit considerable donor-to-donor variability. These shortcomings highlight the need for a reproducible and scalable source of functionally robust DPCs that can yield a potent and standardized secretome.

The paradigm of cell-free regeneration is rooted in the "paracrine hypothesis,"[49] which established that MSCs restore damaged tissues primarily through secreted factors rather than direct engraftment. Secretome-based therapeutics confer unique advantages—lower immune risk, absence of tumorigenicity, enhanced stability, straightforward storage, and clinical scalability.[50] Although MSC- and DPC-derived secretomes have demonstrated some regenerative benefit,[14,51–54] their inconsistent potency underscores the need for molecularly rejuvenated secretome sources.

To address these challenges, we developed a rapid, chemically defined differentiation protocol to generate dermal papilla–like cells from human induced pluripotent stem cells (hiPSCs). Within 8 days, these hiPSC-derived DPCs (hiPSC-DPCs) exhibited robust expression of canonical DP markers and demonstrated strong inductive potency. Conditioned medium collected from hiPSC-DPCs (hiPSC-DPC CM) induced pronounced hair regeneration in depilated mice and ex vivo follicle cultures, triggering anagen re-entry and hair-shaft elongation more effectively than minoxidil. This strategy harnesses the paracrine potential of DPCs while circumventing the immunologic, ethical, and scalability limitations of live-cell transplantation.

A key explanation for the superior efficacy of the hiPSC-DPC secretome lies in its developmental and epigenetic rejuvenation. Primary DPCs from aged or alopecic scalp exhibit features of senescence, oxidative stress, and downregulation of inductive genes such as LEF1, SOX2, and ALP, which compromise their morphogenetic function. In contrast, cellular reprograming resets epigenetic age and restores a developmentally "younger" transcriptional identity. Differentiation of hiPSCs into DPC-like cells re-establishes a youthful signaling phenotype characterized by heightened responsiveness to *Wnt*, BMP, and FGF cues. Consequently, the hiPSC-DPC secretome likely comprises an expanded and balanced spectrum of trophic factors, microRNAs, and EVs cargo that promote angiogenesis, epithelial–mesenchymal communication, and follicular remodeling. The reduced oxidative and inflammatory baseline of these rejuvenated cells may further stabilize their secretory phenotype and enhance functional potency. In parallel, metabolic reprograming may reinforce this regenerative advantage. Hair regeneration is an energy-intensive process demanding tight coordination of redox and nutrient-sensing pathways. hiPSC-DPCs demonstrate elevated glycolytic flux and preserved mitochondrial integrity, facilitating the release of metabolites and cofactors that sustain anabolic and antioxidative activity within the follicular niche. This metabolically "youthful" secretome likely underlies the observed cytoprotective and antioxidative outcomes, intrinsically linking energy metabolism to regenerative efficacy.

Beyond its direct folliculogenic actions, the hiPSC-DPC CM exhibits potent immunomodulatory activity, an essential but often underappreciated determinant of HF regeneration. Proteomic and cytokine profiling revealed enrichment of anti-inflammatory mediators, including interleukin-10 (IL-10), transforming growth factor-β (TGF-β), and prostaglandin-E_2–related enzymes, which collectively suppress pro-inflammatory macrophage activation and promote an M2 reparative phenotype. Concurrent modulation of T-cell-associated cytokines suggests restoration of immune tolerance and re-establishment of regulatory T-cell equilibrium within the follicular environment. Because breakdown of immune privilege and chronic micro-inflammation are hallmarks of both AGA and alopecia areata, such paracrine immunoregulation likely plays a critical role in maintaining long-term follicular stability. By tempering inflammation, mitigating oxidative stress, and preventing autoimmune-like injury, the hiPSC-DPC secretome re-creates an immune-protected, homeostatic niche conducive to sustained hair cycling. Thus, the secretome functions across multiple mechanistic layers—rejuvenating follicular stem-cell signaling, neutralizing androgenic and oxidative insults, and restoring dermal–epithelial immune balance. This multifaceted mechanism distinguishes it from traditional pharmacologic agents such as minoxidil or finasteride, which primarily act by increasing blood flow or inhibiting DHT accumulation.

From a translational perspective, the hiPSC-DPC secretome represents a practical and manufacturable regenerative platform that integrates biological potency with clinical feasibility. Unlike cell-transplantation therapies, this acellular biologic is inherently compatible with Good Manufacturing Practice (GMP) standards, enabling precise quality control and reproducible batch production. The ability to concentrate, lyophilize, or formulate the secretome as a stable preparation supports diverse delivery routes—topical, injectable, or microneedle-assisted—while preserving bioactivity. Its non-living nature minimizes safety concerns related to tumorigenicity or immune

incompatibility, streamlining regulatory approval. Moreover, the self-renewing capacity of hiPSCs provides limitless scalability, supporting affordable, "off-the-shelf" production of pharmaceutical-grade biologics. Collectively, these advantages position the hiPSC-DPC secretome as a next-generation regenerative biologic that merges developmental reprograming with manufacturability, opening a path toward safe, stable, and clinically adaptable cell-free therapeutics for alopecia and related cutaneous disorders.

This study provides the first proof-of-concept demonstration that a secretome derived from hiPSC-induced dermal papilla cells alone—without cell transplantation—is sufficient to restore hair growth and suppress androgenic pathology in vivo, marking a pivotal advance in regenerative dermatology. The mechanistic framework established here may extend well beyond alopecia. Developmental resetting and paracrine rejuvenation achieved through hiPSC differentiation could be harnessed to address a spectrum of dermatologic and regenerative disorders, from chronic wounds to cutaneous aging. Thus, the hiPSC-DPC secretome represents a generalizable strategy for reactivating tissue-specific communication and restoring epithelial–mesenchymal homeostasis.

In summary, hiPSC-derived DPC secretome therapy bridges the gap between drug-based and cell-based approaches. By restoring DPC function through paracrine mechanisms while simultaneously suppressing androgen-driven follicular pathology, this platform establishes a transformative, mechanistically grounded foundation for durable, cell-free treatment of alopecia.

Materials and methods

Cell culture

The hiPSC cell line (CMC-hiPSC-011) was obtained from the Korea National Stem Cell Bank (KSCB), which is part of the Korea National Institute of Health (KNIH), and maintained using TeSR-E8 (STEMCELL Technologies). Human primary DPCs was purchased from Cell Applications (cat# 602-05a) and maintained in Human Hair Follicle Dermal Papilla Cell Growth Medium (Cell Applications). HaCaT was purchased from Procell (cat# CL-0090) and maintained in Dulbecco's Modified Eagle Medium (DMEM, Gibco) supplemented with 10% FBS (ExCell Bio), 1 × MEM Non-Essential Amino Acid (NEAA), 1 × Sodium Pyruvate, and 1 × Antimycotic-Antibiotic (Anti-Anti, Gibco). Human primary DFs was purchased from Cell Applications (cat# 106-05a) and maintained in the same culture medium as HaCaT. Human primary KCs was purchased from Gibco (cat# C0015C) and maintained in EpiLife Medium supplemented with 1 × Human Keratinocyte Growth Supplement (HKGS, Gibco) and 1 × Anti-Anti. Cells were cultured in a humidified incubator at 37°C with 5% CO_2.

Rapid differentiation of hiPSC-DPCs

To initiate the differentiation, hiPSCs were dissociated into single cells using Accutase and cultured with neural lineage restriction (NLR) media containing 20% KnockOut Serum Replacement (KSR, Gibco), 2 μM LDN193189, 10 μM SB431542, and 10 μM Y27632 (SelleckChem) in basal DMEM/F12 (Gibco). After 24 h, the differentiation medium was replaced with neural crest specification (NC) media containing 1 × N2 supplement, 1 × GlutaMAX, 1 × NEAA, 20 ng/ml EGF, 20 ng/ml bFGF (R&D Systems), 20 μM SB431542, and 10 μM Y27632 in Neurobasal medium (Gibco), and the cells were incubated for 3 days. On day 4, the cells were dissociated and re-plated onto 0.2% Gelatin (Sigma-Aldrich)-coated dishes with DPC media containing 10% FBS or 5% Human Platelet Lysate (HPL, Sigma-Aldrich), 20 ng/ml bFGF, 1 × NEAA, and 10 μM Y27632 for 24 h, and the media was changed every 2 days until day 8 using DPC media without inclusion of Y27632.

Preparation of conditioned medium (CM)

The conditioned medium (CM) was prepared by culturing hiPSC-DPCs and hDPCs in basal DMEM/F12 medium for 48 h. After the incubation, the medium was collected and centrifuged at 300×*g* for 10 min at 4°C to remove cellular debris. The supernatant was then sterile-filtered with a 0.22 μm polyethersulfone syringe filter (Sartorius) and stored at −80°C until use.

qRT-PCR

The total RNA was extracted from hiPSCs, hiPSC-NCs, hiPSC-DPCs, and hDPCs using the TRIzol Reagent (Invitrogen) according to the manufacturer's instructions. The concentration and purity of isolated RNA were determined by Nanodrop One Spectrophotometer (Thermo Fisher Scientific), and 1 μg of RNA was subjected to cDNA synthesis using SuperScript IV Reverse Transcriptase (Invitrogen). qRT-PCR was performed using TB Green® Premix Ex Taq (Takara) on a QuantStudio 5 Real-Time PCR System (Applied Biosystems). Relative gene expression levels were calculated using the comparative Ct ($2^{-\Delta\Delta Ct}$) method, normalized to the levels of the housekeeping gene, 18S. The primer sequences of target genes are listed in Supplemental Table 1.

Flow cytometry

Cell suspensions of hiPSC-DPCs and hDPCs were prepared by enzymatic dissociation, followed by fixation using 4% paraformaldehyde (PFA, Santa Cruz) for 10 min at room temperature (RT). The cells were then washed twice with cold phosphate-buffered saline (PBS) containing 2% FBS. For immunolabels of surface markers, 1 million cells were

incubated with 100 µl of APC-conjugated CD44 (BD Biosciences, cat# 559942, 1:5), PE-conjugated CD73 (BD Biosciences, cat# 550257, 1:5), and PE-conjugated CD90 antibodies (BD Biosciences, cat# 555596, 1:20) for 30 min at 4°C in the dark. After repeated washing steps using cold PBS, samples were subsequently analyzed using the CytoFLEX S Flow cytometer analyzer (Beckman Coulter). A minimum of 50,000 live events was recorded for each sample, and gating was set based on unstained controls. The analyses were performed using CytExpert software (v2.6, Beckman Coulter).

Immunocytochemistry

Cells were cultured on Nunc Lab-Tek II Chambered Coverglass (Thermo Fisher Scientific) prior to immunolabelling. After 15 min fixation using 4% PFA, cells were permeabilized with 0.2% Triton X-100 (Thermo Fisher Scientific) for another 15 min at RT, and blocked using 3% bovine serum albumin (BSA, Sigma-Aldrich) for 1 h at RT. Subsequently, the cells were incubated with primary antibodies against Nestin (R&D Systems, cat# MAB1259, 1:250), SMA (Abcam, cat# ab5694, 1:100), Vimentin (Abcam, cat# ab92547, 1:100), Ki67 (Abcam, cat# ab16667, 1:800), and AR (Cell Signaling Technology, cat# 5153, 1:800) overnight at 4°C in blocking buffer. The next day, cells were washed three times with PBST (1% Tween 20 in PBS) and incubated with secondary antibodies, Alexa Fluor 568 Goat anti-rabbit IgG (Invitrogen, cat# A-11011, 1:500) or Alexa Fluor 488 Goat anti-mouse IgG (Invitrogen, cat# A-11001, 1:500) for 1 h at RT in the dark. Cells were further washed three times with PBST and counterstained with VECTASHIELD® Antifade Mounting Medium with DAPI (VectorLabs). All fluorescence images were acquired using a Nikon A1HD25 High Speed and Large Field Confocal Microscope.

Western blot

Cells were harvested and lysed in an ice-cold RIPA buffer supplemented with protease inhibitor (Solarbio). Protein concentrations were quantified using the Pierce BCA protein assay kit (Thermo Fisher Scientific). For each sample, an equal amount of protein was mixed with loading buffer and denatured at 96°C for 10 min. Protein samples were separated on 10% gradient SDS-PAGE gels and transferred to 0.45 µm Nitrocellulose Membrane (Bio-Rad). Membranes were blocked with 5% non-fat dry milk and incubated overnight at 4°C with primary antibodies against the following target proteins: CD133 (Abcam, cat# ab19898, 1:1000), Versican (Invitrogen, PA1-1748A, 1:1000), Akt (Cell Signaling Technology, cat# 4691, 1:1000), Phospho-Akt (Cell Signaling Technology, cat# 4060, 1:1000), GSK (Cell Signaling Technology, cat# 9315, 1:1000), Phospho-GSK (Cell Signaling Technology, cat# 9336, 1:1000), GAPDH (Cell Signaling Technology, cat# 2118, 1:2000). After three times of 5-min washing procedure using Tris-buffered saline with Tween-20 (TBST, Thermo Fisher Scientific), the membranes were incubated with Goat anti-rabbit IgG (H + L) Secondary Antibody, HRP (Invitrogen, cat# 65-6120, 1:2500) or Goat anti-Mouse IgG (H + L) Secondary Antibody, HRP (Invitrogen, cat# 31430, 1:2500) for 1 h at RT. The membranes were washed three times, and protein bands were detected by Pierce ECL western blotting substrate (Thermo Fisher Scientific) and imaged with ChemiDoc Imaging Systems (Bio-Rad). The intensity of protein of each sample was measured and analyzed using ImageJ software (NIH), and the relative protein levels were normalized to the GAPDH loading control.

ALP staining assay

The ALP staining was performed using BCIP/NBT Alkaline Phosphatase Color Development Kit (Beyotime) according to the manufacturer's instructions. Briefly, the cells were fixed with 4% PFA for 15 min at RT and incubated with the freshly prepared ALP staining solution for 30 min at RT in the dark. The reaction was terminated by aspirating the staining solution and thorough washing steps with distilled water. The ALP-stained cells were observed and photographed by a Nikon ECLIPSE Ts2 inverted microscope, and the percentage of stained area was quantified by ImageJ software.

ALP activity assay

ALP activity was measured with Alkaline Phosphatase Activity Assay Kit (Beyotime) according to the manufacturer's instructions. Briefly, cells were lysed with Western and IP Cell Lysis Buffer (Beyotime). After centrifugation at 4°C, the supernatant was collected, and the protein concentrations were quantified using Pierce BCA protein assay kit. The standard curve was generated using the p-nitrophenol standard, and the samples were incubated with chromogenic substrate for 10 min at 37°C. The reaction was terminated by adding the stop solution, and the absorbance at 405 nm was measured with a Varioskan LUX multimode microplate reader (Thermo Fisher Scientific). The ALP activity of each group was normalized with standards and calculated according to the unit definition of ALP. One unit was defined as the amount of ALP required to hydrolyze the p-nitrophenyl phosphate to produce 1 µmol of p-nitrophenol per minute at pH 9.8 and 37℃ in diethanolamine (DEA) buffer.

Animals

All experimental animals were purchased from the Laboratory Animal Research Unit (LARU) of City

University of Hong Kong (CityUHK) and housed in a pathogen-free condition with a 12-h light/dark cycle, and free access to food and water. All animal experiments were approved and complied with the guidelines formulated by the Animal Ethics Committee of CityUHK and the Department of Health in Hong Kong.

In vivo hair regrowth assay

To induce the synchronized entry of hair follicles into the anagen phase of the hair cycle, 7-week-old C57BL/6 mice were depilated 1 day before starting the experiment. The mice were anesthetized, and the hair at the dorsal region was removed by electric clipper and hair removal cream, followed by careful rinsing with water to prevent skin irritation. The depilated mice were randomly divided into groups ($n=5$) for hair regrowth assays. For subcutaneous injection of hiPSC-DPCs, a cell suspension containing 5×10^6 cells/mL and 10 μM Y27632 was prepared. PBS containing 10 μM Y27632 was used as a vehicle control, and 5% minoxidil (Sigma-Aldrich) was employed as a positive control. Treatments for hiPSC-DPCs and vehicle control groups were subcutaneously injected into 10 spots (20 μl/spot/mouse) on the depilated dorsal region on day 0 only, while minoxidil was topically applied every day until day 9. Hair regrowth was monitored and photographed every 5 days. For topical application of CM, 50% hiPSC-DPC CM and 50% hDPC CM in PBS were prepared. PBS was used as a vehicle control, and 5% minoxidil was used as a positive control. All the treatments were topically applied to the depilated dorsal region every day until day 9. For each mouse, 50 μl of treatment was applied per day with a microneedle roller to enhance the absorption. Hair regrowth was monitored and photographed every 2 days, and mice were sacrificed on day 10 for histological analysis.

Histological analysis

The dorsal skin samples of sacrificed mice were fixed with 4% PFA overnight at 4°C and embedded in paraffin blocks. 5 μm thick sections were stained with hematoxylin and eosin (H&E, VectorLabs) for histomorphometry analysis. The key parameters, including the number of hair follicles and the length of hair follicles, were quantified using ImageJ software.

CCK-8 cell proliferation assay

Cell viability and proliferation in response to hiPSC-DPC CM treatments in various conditions were assessed using the Cell Counting Kit-8 (CCK-8, Dojindo). Cells were seeded into 96-well plates at a density of 3000–5000 cells/well, depending on cell types. After overnight cell attachment, the medium was replaced with fresh medium containing various treatments or the vehicle control. After the treatment, 10 μl of CCK-8 solution was added to each well, incubated for 2 h at 37°C, and the absorbance at 450 nm was measured using a microplate reader.

Transwell migration assay

HaCaT and hDF cells were plated on a 24-well culture insert (Corning) at a density of 1×10^5 cells/insert using serum-free medium. At the bottom of the culture insert, serum-containing medium with or without hiPSC-DPC CM was loaded as a chemoattractant. The cells were allowed to migrate for 72 h, fixed with 4% PFA for 15 min at RT, stained with 0.1% Crystal Violet for 15 min at RT, and the unmigrated cells remaining in the upper chamber were removed with a cotton swab. Migrated cells were observed under a Nikon ECLIPSE Ts2 inverted microscope and quantified using ImageJ software.

Scratch migration assay

HaCaT migration was evaluated using a scratch assay with a 2-well culture insert (ibidi). About 3500 cells in 70 μl medium were seeded into each chamber and cultured until confluent. A uniform scratch was created when the chamber was removed, and cells were rinsed gently with DPBS to remove debris. The migration was maintained in a serum-free medium supplemented with either vehicle control, 5% hiPSC-DPC CM, or 10% hiPSC-DPC CM. Images of the wound area were captured at 0, 24, 48, and, and 72 h by Nikon ECLIPSE Ts2 inverted microscope. Wound closure rates were quantified using ImageJ software and presented as a percentage of wound area covered by cells.

Mouse vibrissa hair follicle organ culture

Six-week-old C57BL/6 mice were anesthetized with isoflurane and euthanized via cervical dislocation. Hair follicles were isolated and cultured as previously described.[55] Briefly, follicles were micro-dissected from mystacial pads under a Nikon SMZ745 stereoscopic microscope, and intact hair follicles at the anagen phase were selected and randomly divided into different groups. The hair follicles were transferred to individual wells of a 24-well plate and cultured with William's E medium supplemented with 1× GlutaMAX, 1× Insulin-Transferrin-Selenium (Gibco), 10 ng/ml hydrocortisone (Sigma-Aldrich), and 1× Anti-Anti for 24 h. After stabilization, the culture medium described above was supplemented with vehicle control, 20% hiPSC-DPC CM, and 50% hiPSC-DPC CM for the normal model, and media containing vehicle control, 100 nM DHT (Solarbio), 100 nM DHT + 20% hiPSC-DPC CM, and 100 nM DHT + 50% hiPSC-DPC CM were applied for the androgenetic alopecia model. The treatment was refreshed every 48 h, and the follicles were photographed daily using a Nikon ECLIPSE Ts2 inverted

microscope. Hair shaft and hair bulb length changes were quantified using ImageJ software.

Human hair follicle organ culture

Human scalp skin was obtained from nonbalding areas of patients undergoing hair transplant surgery, with written consent and Institutional Review Board approval from Dankook University Hospital. Human hair follicles were isolated by microdissection under the microscope. Anagen VI hair follicles were chosen for the study. Isolated hair follicles were maintained in William's E medium supplemented with 10 µg/ml insulin (Sigma-Aldrich), 10 ng/ml hydrocortisone (Sigma-Aldrich), 2 mM L-glutamine, 10 U/ml penicillin, 100 µg/ml streptomycin, and 25 µg/ml amphotericin B (Life Technologies). All cultures were incubated at 37°C in an atmosphere of 5% CO_2 and 95% air. The HFs were treated with 20 µM minoxidil or 20% hiPSC-DPC CM for 8 days, and the hair shaft elongation and hair cycle were analyzed using a stereoscopic microscope (Olympus, SZX16)

Proteomics by data-independent acquisition (DIA) mass spectrometry (MS)

The DIA-MS analysis of hiPSC-DPC CM and hDPC CM was performed on a Q-Exactive HF X (Thermo Fisher Scientific). After protein extraction and proteolysis, an equal amount of peptides was extracted from all samples to mix, and the mixture was diluted with mobile phase A (5% ACN pH 9.8) and injected. The Shimadzu LC-20AB HPLC system coupled with a Gemini high pH C18 column (5 µm, 4.6 mm×250 mm) was used. The sample was subjected to the column and then eluted at a flow rate of 1 mL/min by gradient: 5% mobile phase B (95% CAN, pH 9.8) for 10 min, 5%–35% mobile phase B for 40 min, 35%–95% mobile phase B for 1 min, flow Phase B lasted 3 min and 5% mobile phase B equilibrated for 10 min. The elution peak was monitored at a wavelength of 214 nm, and the component was collected every minute. Components were combined into a total of 10 fractions, which were then freeze-dried. Next, the dried peptide samples were reconstituted with mobile phase A (2% ACN, 0.1% FA), centrifuged at 20,000*g* for 10 min, and the supernatant was taken for injection. Separation was carried out by a Thermo UltiMate 3000 UHPLC liquid chromatograph. The sample was first enriched in the trap column and desalted, and then entered a tandem self-packed C18 column (150 µm internal diameter, 1.8 µm column size, 35 cm column length), and separated at a flow rate of 500 nL/min by the following effective gradient: 0–5 min, 5% mobile phase B (98% ACN, 0.1% FA); 5–120 min, mobile phase B linearly increased from 5% to 25%; 120–160 min, mobile phase B rose from 25% to 35%; 160–170 min, mobile phase B rose from 35% to 80%; 170–175 min, 80% mobile phase B; 175–180 min, 5% mobile phase B. The nanoliter liquid phase separation end was directly connected to the tandem mass spectrometer Q-Exactive HF X with DIA (data-independent acquisition) detection mode. The main settings were: ion source voltage 1.9 kV; MS scan range 400–1250 m/z; MS resolution 120,000, MIT 50 ms; 400–1250 m/z was equally divided into 45 continuous windows MS/MS scan. MS/MS collision type HCD, MIT was auto mode. Fragment ions were scanned in Orbitrap, MS/MS resolution 30,000, collision energy was distributed mode: 22.5, 25, 27.5, AGC was 1E6.

Proteomics data analysis

Quantification of peptides and proteins was performed using MSstats software packages. Identification and quantification of peptides and proteins were obtained from the DDA spectral library by deconvolution of the DIA data. The MSstats software package was used to perform differential analysis, followed by functional analysis of the differential proteins. Gene ontology (GO) analysis was conducted to gain insights into the biological functions and processes associated with the differentially expressed genes (DEG). DEGs were identified through a translation of protein ID harvested from statistical analysis of proteomics into gene ID by using Uniprot ID mapping (https://www.uniprot.org/id-mappoing). GO analysis categorized genes into three main categories: molecular function, cellular component, and biological process, to reveal the enriched GO terms in the comparison between hiPSC-DPC CM and hDPC CM. Differentially expressed proteins (DEPs) were determined through one-way ANOVA statistical analysis by MetaboAnalyst (https://www.metaboanalyst.ca/). The DEPs were then subjected to enrichment analysis against the KEGG database (https://www.genome.jp/kegg/). Pathways with a p-value < 0.05 were considered significantly enriched. The pathways that were found to be significantly enriched were then interpreted in the context of hair regeneration. The results of KEGG pathway enrichment analysis are often visualized through bubble plots by using SRPLOT (https://www.bioinformatics.com.cn/en).

Sample preparation for metabolomics

hDPCs from two different sources and hiPSC-DPCs were included for analyzing the cell-secreted metabolites. After the collection of CM, 25 mg samples from each group were weighed and added with magnetic beads into 2 ml centrifuge tubes for extracting the metabolites. About 10 µl of prepared standard consisting of d3-Leucine, 13C9-Phenylalanine, d5-Tryptophan, and 13C3-Progesterone were added with 800 µl precooled extraction buffer which contained methanol (Thermo Fisher Scientific), acetonitrile (Thermo Fisher Scientific) and Milli-Q water with the ratio of 2:2:1. After grinding, the ground samples were stored at −20°C for 2 h

prior to centrifugation at 25,000*g* for 15 min at 4°C. About 600 µl of each sample was transferred into split-new EP tubes for freeze-dry. Next, 120 µl of 50% methanol was put into the dried sample and shaken until completely dissolved. After centrifugation, the supernatant was transferred into a split-new EP tube. About 10 µl of each sample was mixed into QC samples for quality control, and the remaining supernatant was passed to the LC-MS/MS steps.

Metabolomics by ultra-performance liquid chromatography (UPLC) mass spectrometry (MS)

In this experiment, Waters 2777c UPLC (Waters) in series with Q exactive HF high resolution mass spectrometer (Thermo Fisher Scientific) was used for the separation and detection of metabolites. Chromatographic separation was performed on a Waters ACQUITY UPLC BEH C18 column (1.7 µm, 2.1 mm × 100 mm, Waters), and the column temperature was maintained at 45°C. The mobile phase consisted of 0.1% formic acid (A) and acetonitrile (B) in the positive mode, and in the negative mode, the mobile phase consisted of 10 mM ammonium formate (A; Honeywell Fluka) and acetonitrile (B; DIMKA). The gradient conditions were as follows: 0–1 min, 2% B; 1–9 min, 2%–98% B; 9–12 min, 98% B; 12–12.1 min, 98% B–2% B; and 12.1–15 min, 2% B. The flow rate was 0.35 ml/min, and the injection volume was 5 µl. Q Exactive HF was applied to perform primary and secondary mass spectrometry data acquisition. The full scan range was 70–1050 m/z with a resolution of 120,000, and the automatic gain control (AGC) target for MS acquisitions was set to 3e6 with a maximum ion injection time of 100 ms. Top 3 precursors were selected for subsequent MS fragmentation with a maximum ion injection time of 50 ms and resolution of 30000; the AGC was 1e5. The stepped normalized collision energy was set to 20, 40, and 60 eV. ESI parameters were set as follows: sheath gas flow rate was 40, aux gas flow rate was 10, positive-ion mode spray voltage(|KV|) was 3.80, negative-ion mode Spray voltage(|KV|) was 3.20, capillary temperature was 320°C, aux gas heater temperature was 350°C.

Metabolomics data analysis

Off-line data of mass spectrometry was imported into Compound Discoverer 3.3 (Thermo Scientific™) software and analyzed in combination with bmdb (BGI metabolome database), mzcloud database, and ChemSpider online database, which included the information of metabolite peak area and identification results. After that, the obtained data was further processed and analyzed. The result from Compound Discoverer was input into MetaboAnalyst 6.0 for data processing, which included normalization of the data to obtain relative peak areas by Probabilistic Quotient Normalization (PQN)quality control-based robust LOESS signal correction to correct Batch effect, removal of metabolites with a Coefficient of Variation larger than 30% on their Relative peak area in QC Samples. Principal component analysis (PCA) was employed as an unsupervised pattern recognition approach to statistically analyze multidimensional data from three groups and nine samples in total. Taxonomic and functional annotation of the identified metabolites was used to understand the properties of different metabolites. The Human Metabolome Database contains chemical, molecular biology/biochemical, and clinical information of metabolites were referred to support the metabolic pathway search and spectral search. Pathway analysis from KEGG was used to determine numerous metabolic pathways and the relationships between them. Partial Least Squares-Discriminant Analysis (PLS-DA) was a supervised statistical approach to screen the differences between groups.

DCFDA ROS assay

Intracellular levels of ROS were quantified using Reactive Oxygen Species Assay Kit (Beyotime). Cells were seeded in 96-well plates at 8×10^3 cells per well. After 24-h attachment, cultures were treated with serum-free DMEM containing either: (i) vehicle control, (ii) 150 µM H_2O_2 (Sigma-Aldrich), or (iii) 150 µM H_2O_2 plus 20% hiPSC-DPC CM for 30 min. Cells were washed twice with PBS and incubated with 10 µM $DCFH_2$-DA in DMEM for 20 min. Following additional PBS washes, DCF fluorescence intensity was measured with excitation and emission wavelengths of 488 and 535 nm, respectively, using a Varioskan LUX multi-mode microplate reader. Parallel samples were imaged under a Nikon Eclipse Ti2 fluorescence microscope for visualization of ROS intensity levels.

DPPH radical scavenging assay

The 2,2-diphenyl-1-picrylhydrazyl (DPPH) assay was performed to evaluate the free radical scavenging activities of hiPSC-DPC CM. Briefly, DPPH (Sigma-Aldrich) working compound was freshly prepared by dissolving 1.5 mg DPPH in 40.5 ml methanol. About 10%, 20%, 30%, and 50% hiPSC-DPC CM were mixed with the DPPH working solution. PBS and DMEM/F12 were used as negative controls. Five minutes after reaction, the absorbance was measured at 515 nm using a microplate reader. For accurate results, the data from each group was normalized based on the absorbance from PBS or DMEM/F12 controls.

Inflammatory cytokine array

THP-1 cells, cultured in RPMI (supplemented with 10% FBS and 1% Penicillin-Streptomycin), were differentiated

into M0 Macrophages for 72 h with 200 nM phorbol 12-myristate 13-acetate (PMA, Sigma). The culture media were replaced, allowing cells to rest for 24 h. M0 Macrophages were then treated with either RPMI or 100% hiPSC-DPC CM for 48 h, and cell culture supernatant was collected and subjected to cytokine array analysis. The hiPSC-DPC CM was also incubated for 48 h in the absence of cells. To assess cytokine expression profiles in THP-1 differentiated macrophages treated with CM, the Proteome Profiler Human Cytokine Array (Biotechne) was used following the manufacturer's instructions. The ChemiDoc Imaging system (Bio-Rad) was employed to visualize the intensity of each spot, and the Image Lab software (Bio-Rad) was used for analysis.

Statistical analysis

All quantitative data are shown as means ± SEM unless otherwise specified. The statistical differences between the two groups were analyzed by two-tailed Student's *t* tests. The Statistical differences among three or more groups were analyzed by one-way ANOVA with Dunnett's multiple comparisons test. The results were considered statistically significant when the *p*-value was less than 0.05. All statistical analyses were performed using GraphPad Prism 10.2.2 software (GraphPad Software Inc.).

ORCID iDs

Hyesoo Hwangbo https://orcid.org/0009-0007-3052-5042
Aoyang Pu https://orcid.org/0000-0002-4217-4880
Wanyu Tan https://orcid.org/0009-0003-6127-7150
Eunice Dotse https://orcid.org/0000-0002-1118-6942
Yun-Gwi Park https://orcid.org/0000-0002-7139-7637
Sung-Hwan Moon https://orcid.org/0000-0003-1858-0261
In-Rok Oh https://orcid.org/0000-0001-8177-7556
Kwan Ting Chow https://orcid.org/0000-0003-1012-0797
Hae-Won Kim https://orcid.org/0000-0001-6400-6100
Kiwon Ban https://orcid.org/0000-0003-0805-5439

Ethical considerations

All animal experiments were approved and complied with the guidelines formulated by the Animal Ethics Committee of CityUHK (AN-STA-00000592) and the Department of Health in Hong Kong (DH5-24-223). Human scalp skin was obtained from nonbalding areas of patients undergoing hair transplant surgery, with written consent and Institutional Review Board approval from Dankook University Hospital.

Author contributions

Conceptualization: K.B., H.W.K., B.C.P., S.H.M., I.H.C., and K.T.C. Methodology: H.H., A.P., W.T., H.S., E.D., K.T.C., and K.B. Investigation: H.H., A.P., W.T., E.D.,H.S., X.G., Y.G.P., S.J.P., I..R.O., and H.S. Visualization: Y.L. Supervision: K.B., H.W.K. S.H.M., and B.C.P. Writing—original draft: H.H. and A.P. Writing—review & editing: K.B. B.C.P., S.H.M., and H.W.K.

Funding

The authors disclosed receipt of the following financial support for the research, authorship, and/or publication of this article: This work was financially funded by Tung Biomedical Sciences Center, City University of Hong Kong (9609305 to K.B.), Futian Research Project (9609319 to K.B.), ConRes RMG grant (9239089 to K.B.), CityU New Research Initiatives/ Infrastructure Support (9610530 to K.B.), National Research Foundation of Korea grants (RS-2023-00219981 to K.B. and H.W.K.; RS-2021-NR060095, RS-2024-00348908, RS-2023-00220408 to H.W.K.). This research was also supported by the Korean Fund for Regenerative Medicine (KFRM) grant funded by the Ministry of Science and ICT, the Ministry of Health & Welfare (25A0203L1) of Korea grant funded (MSIT, Republic of Korea), and the TIPS program funded by the Ministry of SMEs and Startups (RS2024-00514927).

Declaration of conflicting interests

The authors declared the following potential conflicts of interest with respect to the research, authorship, and/or publication of this article: K.W.B. holds equity in Qstem Co., Ltd. and is an inventor on pending patents related to the methods described in this manuscript. All other authors declare no competing interests.

Data availability statement

All data needed to evaluate the conclusions in the paper are present in the paper and/or the Supplemental Materials.

Supplemental material

Supplemental material for this article is available online.

References

1. Alzoabi NM, Alsharif HM Sr, Alawami AM, et al. Assessing the impact of alopecia on quality of life, depression, and self-esteem in Saudi Arabia. *Cureus* 2023; 15: e49864. https://doi.org/10.7759/cureus.49864
2. Liu Y, Tosti A, Wang ECE, et al. Androgenetic alopecia. *Nat Rev Dis Primers* 2025; 11: 73.
3. Rossi A, Cantisani C, Melis L, et al. Minoxidil use in dermatology, side effects and recent patents. *Recent Pat Inflamm Allergy Drug Discov* 2012; 6: 130–136.
4. Irwig MS and Kolukula S. Persistent sexual side effects of finasteride for male pattern hair loss. *J Sex Med* 2011; 8: 1747–1753.
5. Gupta AK, Lyons DC and Daigle D. Progression of surgical hair restoration techniques. *J Cutan Med Surg* 2015; 19: 17–21.
6. Driskell RR, Clavel C, Rendl M, et al. Hair follicle dermal papilla cells at a glance. *J Cell Sci* 2011; 124: 1179–1182.
7. Zhang H-L, Qiu X-X and Liao X-H. Dermal papilla cells: from basic research to translational applications. *Biology* 2024; 13: 842.
8. Madaan A, Verma R, Singh AT, et al. Review of hair follicle dermal papilla cells as in vitro screening model for hair growth. *Int J Cosmet Sci* 2018; 40: 429–450.
9. Inui S and Itami S. Molecular basis of androgenetic alopecia: from androgen to paracrine mediators through dermal papilla. *J Dermatol Sci* 2011; 61(1): 1–6.

10. Hull SM, Nutbrown M, Pepall L, et al. Immunohistologic and ultrastructural comparison of the dermal papilla and hair follicle bulb from "active" and "normal" areas of alopecia areata. *J Investig Dermatol* 1991; 96: 673–681.
11. Ohyama M, Kobayashi T, Sasaki T, et al. Restoration of the intrinsic properties of human dermal papilla in vitro. *J Cell Sci* 2012; 125: 4114–4125.
12. Higgins CA, Chen JC, Cerise JE, et al. Microenvironmental reprogramming by three-dimensional culture enables dermal papilla cells to induce de novo human hair-follicle growth. *Proc Natl Acad Sci* 2013; 110: 19679–19688.
13. Ouji Y, Ishizaka S and Yoshikawa M. Dermal papilla cells serially cultured with Wnt-10b sustain their hair follicle induction activity after transplantation into nude mice. *Cell Transplant* 2012; 21: 2313–2324.
14. Hu S, Li Z, Lutz H, et al. Dermal exosomes containing miR-218-5p promote hair regeneration by regulating β-catenin signaling. *Sci Adv* 2020; 6: eaba1685. https://doi.org/10.1126/sciadv.aba1685
15. Gnedeva K, Vorotelyak E, Cimadamore F, et al. Derivation of hair-inducing cell from human pluripotent stem cells. *PLoS One* 2015; 10: e0116892.
16. Veraitch O, Mabuchi Y, Matsuzaki Y, et al. Induction of hair follicle dermal papilla cell properties in human induced pluripotent stem cell-derived multipotent LNGFR(+)THY-1(+) mesenchymal cells. *Sci Rep* 2017; 7: 42777.
17. Riabinin A, Kalabusheva E, Khrustaleva A, et al. Trajectory of hiPSCs derived neural progenitor cells differentiation into dermal papilla-like cells and their characteristics. *Sci Rep* 2023; 13: 14213.
18. Zhou L, Wang H, Jing J, et al. Regulation of hair follicle development by exosomes derived from dermal papilla cells. *Biochem Biophys Res Commun* 2018; 500: 325–332.
19. Kwack MH, Seo CH, Gangadaran P, et al. Exosomes derived from human dermal papilla cells promote hair growth in cultured human hair follicles and augment the hair-inductive capacity of cultured dermal papilla spheres. *Exp Dermatol* 2019; 28: 854–857.
20. Wong CE, Paratore C, Dours-Zimmermann MT, et al. Neural crest-derived cells with stem cell features can be traced back to multiple lineages in the adult skin. *J Cell Biol* 2006; 175: 1005–1015.
21. Jinno H, Morozova O, Jones KL, et al. Convergent genesis of an adult neural crest-like dermal stem cell from distinct developmental origins. *Stem Cells* 2010; 28: 2027–2040. https://doi.org/10.1002/stem.525
22. Zhu Q, Li M, Yan C, et al. Directed differentiation of human embryonic stem cells to neural crest stem cells, functional peripheral neurons, and corneal keratocytes. *Biotechnol J* 2017; 12: 1700067. https://doi.org/10.1002/biot.201700067
23. Chambers SM, Fasano CA, Papapetrou EP, et al. Highly efficient neural conversion of human ES and iPS cells by dual inhibition of SMAD signaling. *Nat Biotechnol* 2009; 27: 275–280. https://doi.org/10.1038/nbt.1529
24. Garcez RC, Teixeira BL, Schmitt Sdos S, et al. Epidermal growth factor (EGF) promotes the in vitro differentiation of neural crest cells to neurons and melanocytes. *Cell Mol Neurobiol* 2009; 29: 1087–1091. https://doi.org/10.1007/s10571-009-9406-2
25. Bak SS, Kwack MH, Shin HS, et al. Restoration of hair-inductive activity of cultured human follicular keratinocytes by co-culturing with dermal papilla cells. *Biochem Biophys Res Commun* 2018; 505: 360–364.
26. Kang BM, Kwack MH, Kim MK, et al. Sphere formation increases the ability of cultured human dermal papilla cells to induce hair follicles from mouse epidermal cells in a reconstitution assay. *J Investig Dermatol* 2012; 132: 237–239.
27. Ito Y, Hamazaki TS, Ohnuma K, et al. Isolation of murine hair-inducing cells using the cell surface marker prominin-1/CD133. *J Investig Dermatol* 2007; 127: 1052–1060.
28. Taghiabadi E, Nilforoushzadeh MA and Aghdami N. Maintaining hair inductivity in human dermal papilla cells: a review of effective methods. *Skin Pharmacol Physiol* 2020; 33: 280–292.
29. Kishimoto J, Soma T, Burgeson R, et al. Versican expression by dermal papilla-regenerated hair follicles – a promising tool for hair-regrowth products. *Int J Cosmet Sci* 2004; 26: 165–166.
30. Lee S-H, Yoon J, Shin SH, et al. Valproic acid induces hair regeneration in murine model and activates alkaline phosphatase activity in human dermal papilla cells. *PLoS One* 2012; 7: e34152.
31. Kwack MH, Jang YJ, Won GH, et al. Overexpression of alkaline phosphatase improves the hair-inductive capacity of cultured human dermal papilla spheres. *J Dermatol Sci* 2019; 95: 126–129.
32. van Beek N, Bodó E, Kromminga A, et al. Thyroid hormones directly alter human hair follicle functions: anagen prolongation and stimulation of both hair matrix keratinocyte proliferation and hair pigmentation. *J Clin Endocrinol Metab* 2008; 93: 4381–4388.
33. Choi BY. Targeting Wnt/β-catenin pathway for developing therapies for hair loss. *Int J Mol Sci* 2020; 21: 4915.
34. Choi YS, Zhang Y, Xu M, et al. Distinct functions for Wnt/β-catenin in hair follicle stem cell proliferation and survival and interfollicular epidermal homeostasis. *Cell Stem Cell* 2013; 13: 720–733.
35. Hendrix S, Handjiski B, Peters EM, et al. A guide to assessing damage response pathways of the hair follicle: lessons from cyclophosphamide-induced alopecia in mice. *J Investig Dermatol* 2005; 125: 42–51.
36. Milner Y, Sudnik J, Filippi M, et al. Exogen, shedding phase of the hair growth cycle: characterization of a mouse model. *J Investig Dermatol* 2002; 119: 639–644.
37. Ahn S-Y, Pi LQ, Hwang ST, et al. Effect of IGF-I on hair growth is related to the anti-apoptotic effect of IGF-I and up-regulation of PDGF-A and PDGF-B. *Ann Dermatol* 2012; 24: 26–31.
38. Wang N, Zhang W, Zhong Z, et al. FGF7 secreted from dermal papillae cell regulates the proliferation and differentiation of hair follicle stem cell. *J Integr Agric* 2025; 24: 3583–3597.
39. Estrach S, Ambler CA, Lo Celso CL, et al. Jagged 1 is a β-catenin target gene required for ectopic hair follicle formation in adult epidermis. 2006.
40. Wang X, Chen H, Tian R, et al. Macrophages induce AKT/β-catenin-dependent lgr5+ stem cell activation and

hair follicle regeneration through TNF. *Nat Commun* 2017; 8: 14091.
41. Wang G, Sweren E, Andrews W, et al. Commensal microbiome promotes hair follicle regeneration by inducing keratinocyte HIF-1α signaling and glutamine metabolism. *Sci Adv* 2023; 9: eabo7555.
42. Du F, Li J, Zhang S, et al. Oxidative stress in hair follicle development and hair growth: signalling pathways, intervening mechanisms and potential of natural antioxidants. *J Cell Mol Med* 2024; 28: e18486.
43. Davis MG, Piliang MP, Bergfeld WF, et al. Scalp application of antioxidants improves scalp condition and reduces hair shedding in a 24-week randomized, double-blind, placebo-controlled clinical trial. *Int J Cosmet Sci* 2021; 43: S14–S25.
44. Tao N, Sun Q, Ying Y, et al. Dermal T cell immunity and key regulatory signaling pathways: Implications in immune-mediated alopecia and hair regeneration. *Genes Dis* 2025; 12: 101518.
45. Song X, Shi Y, You J, et al. D-4F, an apolipoprotein AI mimetic, suppresses IL-4 induced macrophage alternative activation and pro-fibrotic TGF-β1 expression. *Pharm Biol* 2019; 57: 470–476.
46. Han X, Kitamoto S, Lian Q, et al. Interleukin-10 facilitates both cholesterol uptake and efflux in macrophages. *J Biol Chem* 2009; 284: 32950–32958.
47. Blauenfeldt T, Petrone L, Del Nonno F, et al. Interplay of DDP4 and IP-10 as a potential mechanism for cell recruitment to tuberculosis lesions. *Front Immunol* 2018; 9: 1456.
48. Dong TR, Li YJ, Jin SY, et al. Progress on mitochondria and hair follicle development in androgenetic alopecia: relationships and therapeutic perspectives. *Stem Cell Res Ther* 2025; 16: 44. https://doi.org/10.1186/s13287-025-04182-z
49. Gnecchi M, He H, Liang OD, et al. Paracrine action accounts for marked protection of ischemic heart by Akt-modified mesenchymal stem cells. *Nat Med* 2005; 11: 367–368. https://doi.org/10.1038/nm0405-367
50. Gunawardena TNA, Rahman MT, Abdullah BJJ, et al. Conditioned media derived from mesenchymal stem cell cultures: the next generation for regenerative medicine. *J Tissue Eng Regen Med* 2019; 13: 569–586. https://doi.org/10.1002/term.2806
51. Zhang H, Zhu N-X, Huang K, et al. ITRAQ-based quantitative proteomic comparison of early- and late-passage human dermal papilla cell secretome in relation to inducing hair follicle regeneration. *PLoS One* 2016; 11: e0167474. https://doi.org/10.1371/journal.pone.0167474
52. Chen Y, Huang J, Chen R, et al. Sustained release of dermal papilla-derived extracellular vesicles from injectable microgel promotes hair growth. *Theranostics* 2020; 10: 1454–1478. https://doi.org/10.7150/thno.39566
53. Kazi T, Nagata A, Nakagawa T, et al. Dermal papilla cell-derived extracellular vesicles increase hair inductive gene expression in adipose stem cells via β-Catenin activation. *Cells* 2022; 11: 202.
54. Ru Z, Wu Y, Qu Q, et al. Dermal papilla cells-conditioned medium attenuates oxidative stress-induced senescence via ferroptosis inhibition. *Sci Rep* 2025; 15: 24789. https://doi.org/10.1038/s41598-025-08968-2
55. Philpott MP, Green MR and Kealey T. Rat hair follicle growth in vitro. *Br J Dermatol* 1992; 127: 600–607. https://doi.org/10.1111/j.1365-2133.1992.tb14873.x